



# tRNA-m<sup>1</sup>A modification promotes T cell expansion via efficient MYC protein synthesis

Yongbo Liu<sup>1,2,14</sup>, Jing Zhou<sup>1,2,3,14</sup>, Xiaoyu Li<sup>4,14</sup>, Xiaoting Zhang<sup>5,14</sup>, Jintong Shi<sup>1,14</sup>, Xuefei Wang<sup>1,2</sup>, Hao Li<sup>6</sup>, Shan Miao<sup>1,2</sup>, Huifang Chen<sup>1,7</sup>, Xiaoxiao He<sup>8</sup>, Liting Dong<sup>5,9</sup>, Gap Ryol Lee<sup>10</sup>, Junke Zheng<sup>8</sup>, Ru-Juan Liu<sup>6</sup>, Bing Su<sup>1,2</sup>, Youqiong Ye<sup>1</sup>, Richard A. Flavell<sup>3,11</sup>✉, Chengqi Yi<sup>5,9,12</sup>✉, Yuzhang Wu<sup>1,7</sup>✉ and Hua-Bing Li<sup>1,2,7,13</sup>✉

**Naive T cells undergo radical changes during the transition from dormant to hyperactive states upon activation, which necessitates de novo protein production via transcription and translation. However, the mechanism whereby T cells globally promote translation remains largely unknown. Here, we show that on exit from quiescence, T cells upregulate transfer RNA (tRNA) m<sup>1</sup>A58 ‘writer’ proteins TRMT61A and TRMT6, which confer m<sup>1</sup>A58 RNA modification on a specific subset of early expressed tRNAs. These m<sup>1</sup>A-modified early tRNAs enhance translation efficiency, enabling rapid and necessary synthesis of MYC and of a specific group of key functional proteins. The MYC protein then guides the exit of naive T cells from a quiescent state into a proliferative state and promotes rapid T cell expansion after activation. Conditional deletion of the *Trmt61a* gene in mouse CD4<sup>+</sup> T cells causes MYC protein deficiency and cell cycle arrest, disrupts T cell expansion upon cognate antigen stimulation and alleviates colitis in a mouse adoptive transfer colitis model. Our study elucidates for the first time, to our knowledge, the in vivo physiological roles of tRNA-m<sup>1</sup>A58 modification in T cell-mediated pathogenesis and reveals a new mechanism of tRNA-m<sup>1</sup>A58-controlled T cell homeostasis and signal-dependent translational control of specific key proteins.**

CD4<sup>+</sup> T cells constitute the major arm of adaptive immunity. Upon antigen stimulation, naive T cells undergo rapid and profound changes to exit from the quiescent state, followed by the massive clonal expansion and differentiation that is essential for an adequate immune defense<sup>1–4</sup>. T cells meet such massive bioenergetic and biosynthetic demands by rapidly increasing protein synthesis at the transcriptional, posttranscriptional, and translational levels<sup>5–7</sup>. It is well documented that one of the major strategies of the cells is to produce more RNAs and thus more proteins at the transcriptional level<sup>8</sup>. However, this mechanism may not be sufficient at the early stage of T cell activation, given the need for massive expansion of cell size and number during a short time window. Therefore, we postulate that another crucial strategy used by T cells could be fully utilizing the existing finite pool of messenger RNAs (mRNAs) by enhancing translation efficiency (TE).

Translational regulation occurs at the initiation, elongation and termination steps. In these steps, tRNA decoding has a fundamental role. There are more than 400 tRNA genes in the human genome, more than 200 of which are usually expressed in each cell<sup>9</sup>. tRNAs have long been thought to affect translation via their structures and interactions with the corresponding mRNA codons. Their

regulation is closely related to diverse tRNA chemical modifications, which have been the subject of numerous in vitro studies<sup>10–13</sup>. Mammalian tRNAs are the most highly modified RNA molecules in cells<sup>14,15</sup>. On average, they contain 14 modified nucleotides per molecule<sup>16,17</sup>. tRNA modifications have multifaceted roles that involve control, decoding, aminoacylation efficiency and fidelity, in vivo stability and intracellular localization<sup>10–13</sup>. One such evolutionarily conserved epitranscriptomic mark is N<sup>1</sup>-methyladenosine (m<sup>1</sup>A), which is typically found at position 58 of a tRNA and is catalyzed by the tRNA methyltransferases TRMT61A and TRMT6<sup>18,19</sup>. It has been reported that TRMT6- and TRMT61A-mediated tRNA-m<sup>1</sup>A58 modification enhances translation initiation and elongation<sup>20–22</sup>. However, the in vivo biological functions of tRNA-m<sup>1</sup>A58 in immunity have remained completely unknown.

Here, we observe that the gene expression of *Trmt61a* and *Trmt6* increase rapidly upon T cell activation, concomitant with enhanced expression of tRNA subsets. Specific deletion of *Trmt61a* or *Trmt6* in T cells leads to defective T cell expansion, which alleviates colitis in a T cell-mediated adoptive transfer colitis model. Mechanistically, TRMT61A-mediated tRNA-m<sup>1</sup>A58 installation on a subset of early upregulated tRNAs is required to ensure efficient

<sup>1</sup>Shanghai Institute of Immunology, State Key Laboratory of Oncogenes and Related Genes, Shanghai Jiao Tong University School of Medicine, Shanghai, China. <sup>2</sup>Shanghai Jiao Tong University School of Medicine-Yale Institute for Immune Metabolism, Shanghai Jiao Tong University School of Medicine, Shanghai, China. <sup>3</sup>Department of Immunobiology, Yale University School of Medicine, New Haven, CT, USA. <sup>4</sup>Department of Biochemistry and Department of Gastroenterology of the Second Affiliated Hospital, Zhejiang University School of Medicine, Hangzhou, China. <sup>5</sup>State Key Laboratory of Protein and Plant Gene Research, School of Life Sciences, Peking University, Beijing, China. <sup>6</sup>School of Life Science and Technology, ShanghaiTech University, Shanghai, China. <sup>7</sup>Chongqing International Institute for Immunology, Chongqing, China. <sup>8</sup>Hongqiao International Institute of Medicine, Shanghai Tongren Hospital, Key Laboratory of Cell Differentiation and Apoptosis of Chinese Ministry of Education, Faculty of Basic Medicine, Shanghai Jiao Tong University School of Medicine, Shanghai, China. <sup>9</sup>Peking-Tsinghua Center for Life Sciences, Peking University, Beijing, China. <sup>10</sup>Department of Life Science, Sogang University, Seoul, Republic of Korea. <sup>11</sup>Howard Hughes Medical Institute, Yale University School of Medicine, New Haven, CT, USA. <sup>12</sup>Department of Chemical Biology and Synthetic and Functional Biomolecules Center, College of Chemistry and Molecular Engineering, Peking University, Beijing, China. <sup>13</sup>Department of Geriatrics, Medical Center on Aging of Ruijin Hospital, Shanghai Jiao Tong University School of Medicine, Shanghai, China. <sup>14</sup>These authors contributed equally: Yongbo Liu, Jing Zhou, Xiaoyu Li, Xiaoting Zhang, Jintong Shi. ✉e-mail: [richard.flavell@yale.edu](mailto:richard.flavell@yale.edu); [chengqi.yi@pku.edu.cn](mailto:chengqi.yi@pku.edu.cn); [wuyuzhang@iicq.vip](mailto:wuyuzhang@iicq.vip); [huabing.li@shsmu.edu.cn](mailto:huabing.li@shsmu.edu.cn)

translation of a group of key proteins for T cell proliferation, especially MYC protein, which propels T cells into mitosis and complete cell cycles. Collectively, these results demonstrate that tRNA-m<sup>1</sup>A58 methylation serves as a translational checkpoint that constitutes an important mechanism responsible for the rapid synthesis of specific key functional proteins to promote T cell expansion.

## Results

**Translation control is activated during T cell activation.** Upon T cell receptor (TCR) stimulation, naive CD4<sup>+</sup> T cells exit quiescent state and then rapidly go through different cellular stages through sequential reprogramming, including early signaling activation (0–6 h), metabolic reprogramming (6–12 h), pre-cell-cycling (12–24 h) and proliferation (24–72 h)<sup>23,24</sup>. During this activation process, the tRNA pool decodes genetic information during translation and thus may exert crucial functions. To systematically examine the tRNA expression dynamics required for T cell activation, we isolated naive CD4<sup>+</sup> T cells from the spleens of wild-type (WT) mice, activated them with anti-CD3 and anti-CD28 antibodies for 0, 6, 18 and 48 h in vitro, and purified these time-point tRNAs for tRNA sequencing (Fig. 1a). We observed that those tRNA transcripts displayed differential expression profiles, which could be classified into six clusters (Fig. 1b). tRNAs in cluster T1 to cluster T4 were upregulated, whereas those in cluster T5 and cluster T6 displayed random patterns. Specifically, cluster T1 showed early and pronounced upregulation at 6 h and then gradual downregulation, whereas cluster T2 showed upregulation at 6 h and even more marked upregulation at 18 h. This dynamic expression of tRNAs indicates their intricate physiological regulation and potential functions during T cell activation.

In parallel, to systematically examine the molecular components required for T cell expansion, we isolated naive CD4<sup>+</sup> T cells from the spleens of WT mice, activated them with anti-CD3 and anti-CD28 antibodies for 0, 3, 6 and 18 h in vitro, and purified these time-point RNAs for sequencing (Fig. 1a). Kyoto Encyclopedia of Genes and Genomes (KEGG) pathway classification analysis showed that translation event was the most active process in early T cell activation (Fig. 1c), implying that translational control might have an important role in T cells during this process. As transcription is thought to be the most important process during T cell activation, we analyzed transcription and translation genes in parallel. Transcription and translation genes could be classified into five subsets based on mRNA expression profiles (Fig. 1d), suggesting a sequential regulatory program during T cell activation.

Beyond changes in expression levels, primary tRNA transcripts undergo a series of important maturation steps<sup>25–27</sup>. In addition, to support high mRNA-decoding efficiency, the new tRNAs need to be equipped with numerous chemical modifications<sup>28</sup>. Indeed, we observed a notable upregulation of genes related to tRNA processing and tRNA modification in the cluster mA1, consistent with the expression dynamics of cluster T1 and T2 tRNAs (Fig. 1e). Given the importance of TRMT6- and TRMT61A-mediated tRNA-m<sup>1</sup>A58 methylation in controlling tRNA decoding efficiency<sup>9,14</sup> and the lack of in vivo functional studies, we focused on tRNA-m<sup>1</sup>A58 ‘writer’ genes *Trmt61a* and *Trmt6*. Using real-time quantitative polymerase chain reaction (qPCR), we confirmed that mRNA levels of *Trmt61a* and *Trmt6* increased upon T cell activation (Fig. 1f), indicating that tRNA-m<sup>1</sup>A58 modification may be an important translational control in the modulation of T cell activation.

We next explored the potential upstream signaling pathways that might regulate the activation of *Trmt61a* and related tRNA-processing genes. As TCR signaling, interleukin (IL)-2 signaling and IL-7 signaling are the major early pathways for T cell activation, we systematically analyzed the available published T cell chromatin immunoprecipitation (ChIP) sequencing datasets for the major transcription factors downstream of these three signaling

pathways (Extended Data Fig. 1a–c)<sup>29–32</sup>. We found that c-JUN and FOSL2 downstream of TCR signaling bound to the *Trmt61a* gene region, as validated by ChIP–qPCR assay (Extended Data Fig. 1c,d). Notably, FOSL2 and c-JUN were in cluster mB2 and were upregulated early at 3 h postactivation, whereas *Trmt6* and *Trmt61a* of cluster mA1 started to be upregulated from 6 h postactivation, indicating that TCR signaling is likely to activate TRMT6- and TRMT61A-mediated tRNA processing (Fig. 1d).

Next, we performed tRNA methylation sequencing to detect tRNA methylation levels in T cells and cells of various tissues. We found that all common tRNA methylations detected, including N<sup>1</sup>-methyladenosine at position 58 of a tRNA (m<sup>1</sup>A58), N<sup>1</sup>-methylguanosine at position 9 of a tRNA (m<sup>1</sup>G9), N<sup>1</sup>-methylguanosine at position 37 of a tRNA (m<sup>1</sup>G37) and 3-methylcytidine (m<sup>3</sup>C), were maintained at constant levels during T cell activation and in the other cell types (Fig. 1g and Extended Data Fig. 1e), implying the conservation and functional importance of these tRNA methylations. Notably, the tRNA-m<sup>1</sup>A58 modification occurred at a much higher level than the other methylation types. Taken together, these data led us to hypothesize that early upregulated TRMT6 and TRMT61A, induced by TCR signaling, methylate a group of early tRNAs at tRNA-m<sup>1</sup>A58 to enhance the TE of certain proteins for T cell activation.

## TRMT61A ensures the normal immune function of CD4<sup>+</sup> T cells.

To study the in vivo immune function of tRNA-m<sup>1</sup>A58, we generated conditional knockout (KO) mice for tRNA-m<sup>1</sup>A58 ‘writer’ gene *Trmt61a*, which were crossed with *Cd4<sup>Cre</sup>* mice to obtain *Trmt61a<sup>flox/flox</sup> Cd4<sup>Cre</sup>* (*Trmt61a*-KO) mice (Extended Data Fig. 2a). Of note, these mice expressed the *Cre* transgene under the control of the *Cd4* enhancer–promoter–silencer cassette (*Cd4-Cre*), which causes *Trmt61a* gene deletion in CD4 and CD8 double- or single-positive thymocytes. We confirmed that *Trmt61a* mRNA and protein expression were specifically deleted in CD4<sup>+</sup> T cells from *Trmt61a<sup>flox/flox</sup> Cd4<sup>Cre</sup>* mice, in contrast to WT littermate controls (Fig. 2a and Extended Data Fig. 2b). Concomitantly, global tRNA-m<sup>1</sup>A58 modification levels but not tRNA expression levels in *Trmt61a*-KO CD4<sup>+</sup> T cells were decreased compared with those of WT cells (Fig. 2b,c and Extended Data Fig. 2c,d). At steady state, WT and *Trmt61a*-KO mice exhibited similar compositions of T cell subsets in the thymus (Extended Data Figs. 2e and 3a), suggesting that *Trmt61a* deficiency does not disrupt thymic T cell development. However, characterization of T cell functional populations revealed that T cell activation was abnormal in peripheral lymphatic organs from *Trmt61a*-KO mice, as judged by a significant decrease in the proportions of previously activated T cells in the spleen and lymph nodes compared with those of WT mice (Extended Data Figs. 2f–j and 3b). Of note, numbers of both total CD4<sup>+</sup> T and CD8<sup>+</sup> T cells, as well as those of naive CD4<sup>+</sup> T and CD8<sup>+</sup> T cells, were increased in the lymph nodes but decreased in the spleen of *Trmt61a*-KO mice, consistent with a typical observed spontaneous colitis due to disrupted T cell homeostasis.

We used an adoptive transfer colitis model to further evaluate the effects of TRMT61A on the adaptive immune function of CD4<sup>+</sup> T cells in vivo. Naive CD4<sup>+</sup> T cells were purified by fluorescence activated cell sorting (FACS) and then transferred into *Rag2<sup>-/-</sup>* mice, which lack T and B cells. Naive CD4<sup>+</sup> T cells normally undergo uncontrolled rapid homeostatic proliferation and expansion in an in vivo microenvironment, resulting in colitis<sup>33</sup>. Accordingly, we adoptively transferred WT or *Trmt61a*-KO CD4<sup>+</sup>CD25<sup>+</sup>CD45RB<sup>hi</sup> naive T cells into *Rag2<sup>-/-</sup>* mice. Indeed, *Rag2<sup>-/-</sup>* recipient mice receiving WT naive T cells began losing weight in the fifth week after transfer and developed severe colitis characterized by diarrhea or loose stools, piloerection and reduced physical activity (Fig. 2d,e). Endoscopic and pathologic examination documented colon tissue damage and degeneration (Fig. 2f and Extended Data Fig. 3c,d). Hematoxylin and eosin staining and immunohistochemistry

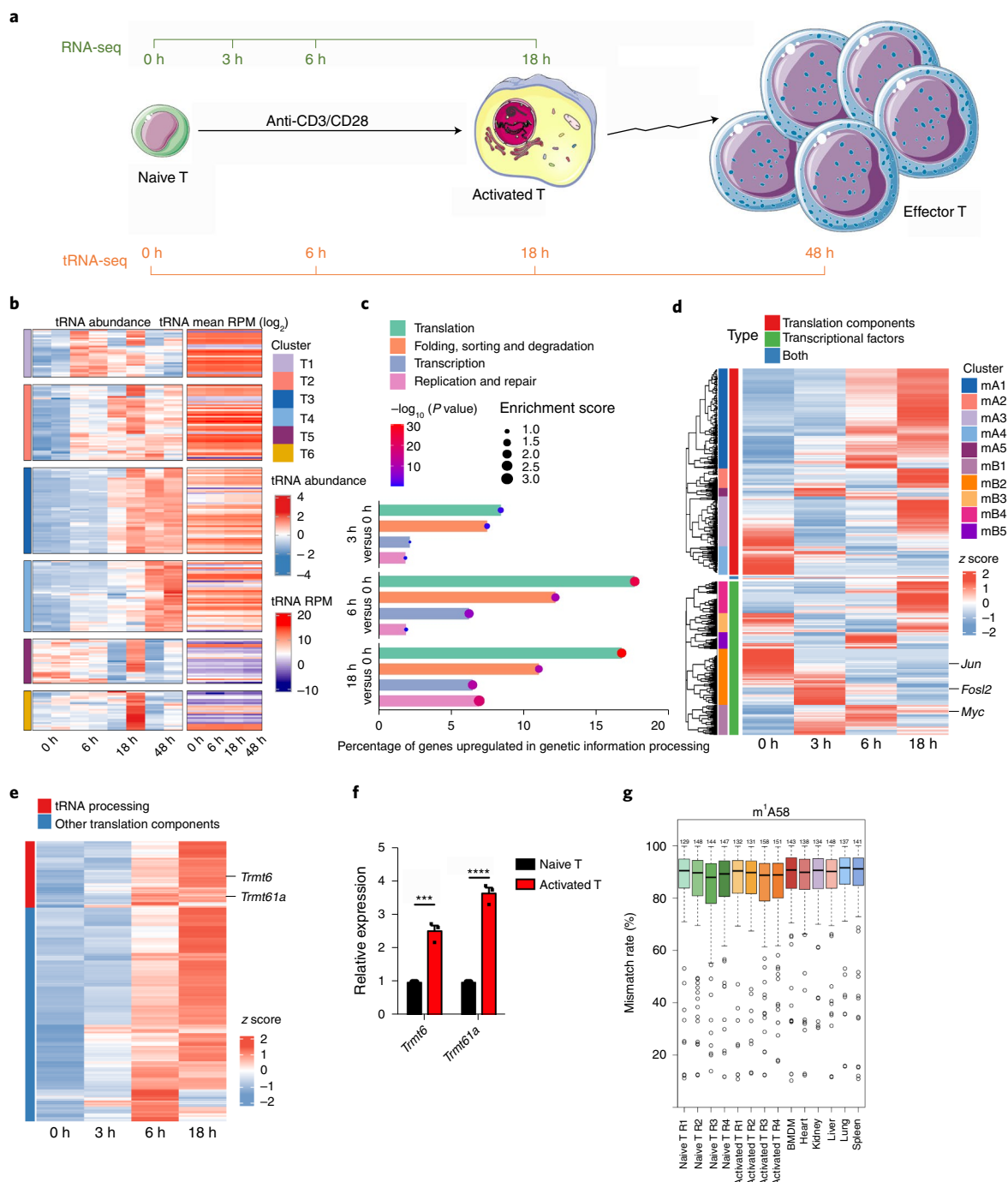


**Fig. 1 | Translation control is activated during T cell activation.** **a**, Schematic depicting RNA sequencing (RNA-seq) and tRNA sequencing (tRNA-seq) assays. **b**, Naive CD4<sup>+</sup> T cells were activated with 5  $\mu\text{g ml}^{-1}$  anti-CD3 antibody and 2  $\mu\text{g ml}^{-1}$  anti-CD28 antibody for 0, 6, 18 and 48 h. After tRNA-seq, the dynamic expression changes of tRNAs in different groups were identified. RPM, reads per million mapped reads. **c**, Naive CD4<sup>+</sup> T cells were activated for 0, 3, 6 and 18 h. After RNA-seq and KEGG pathway classification analysis of these cells at different time points, pathways involved in genetic information processing were identified, and the percentages of genes significantly upregulated in different pathways were also determined. Hypergeometric test (without adjustments) was used. **d**, The expression of genes related to translation and transcription factors in different functional groups was identified according to the RNA-seq results. **e**, Expression of genes related to translation in cluster mA1. **f**, Levels of *Trmt6* and *Trmt61a* mRNAs were analyzed by real-time PCR in naive CD4<sup>+</sup> T cells and in vitro activated CD4<sup>+</sup> T cells (6 h). Error bars represent mean  $\pm$  s.e.m.;  $n = 3$  biologically independent samples from three independent experiments. \*\*\* $P = 0.0008$ , \*\*\*\* $P < 0.0001$ ; two-tailed, unpaired *t*-test. **g**, Quantification of m<sup>1</sup>A58/A58 in total tRNA purified from naive CD4<sup>+</sup> T cells, in vitro activated CD4<sup>+</sup> T cells (24 h), bone marrow-derived macrophages (BMDMs), heart, kidney, liver, lung and spleen by tRNA-seq.  $n = 2$  biologically independent animals. Data are shown as box plots (the value of  $n$  is displayed above boxes; boxes show median, upper and lower quartiles; whiskers show 1.5 $\times$  interquartile range (IQR) on either side; and points show outliers).

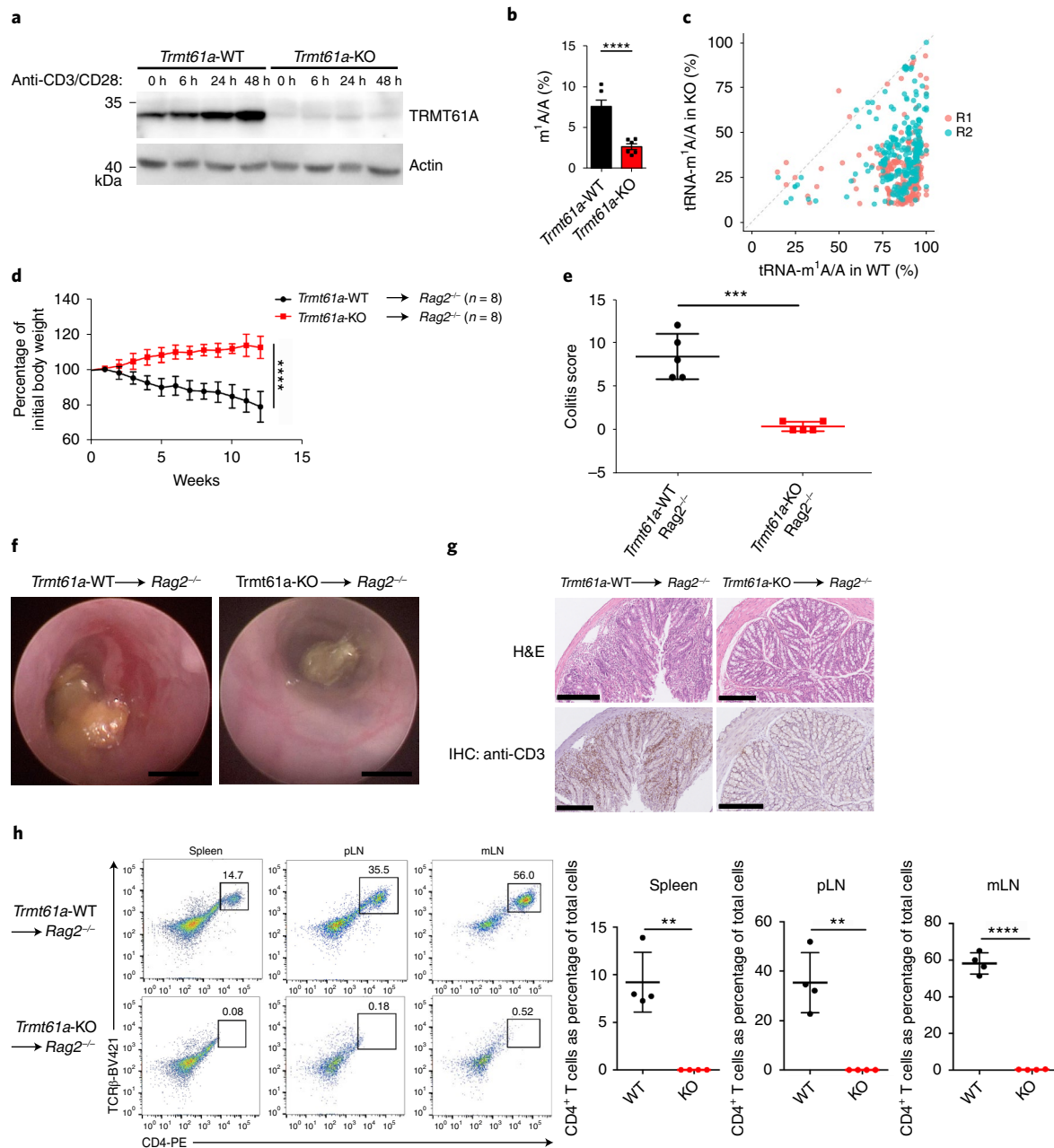


**Fig. 2 | TRMT61A ensures the normal immune function of CD4<sup>+</sup> T cells.** **a**, TRMT61A protein levels in *Trmt61a*-KO and WT naive CD4<sup>+</sup> T cells stimulated with anti-CD3 and anti-CD28 antibodies for 0, 6, 24 and 48 h were quantified by immunoblotting. Representative data of three independent experiments are shown. **b**, Quantification of the m<sup>1</sup>A/A ratio in total tRNA purified from *Trmt61a*-KO and WT activated CD4<sup>+</sup> T cells (24 h) by liquid chromatography with mass spectrometry. Error bars represent mean  $\pm$  s.e.m.,  $n = 6$  biologically independent samples. \*\*\*\* $P < 0.0001$ ; two-tailed, unpaired  $t$ -test. **c**, tRNA-m<sup>1</sup>A sequencing detection of the m<sup>1</sup>A58 modification level of each tRNA in activated *Trmt61a*-KO CD4<sup>+</sup> T cells and WT CD4<sup>+</sup> T cells. Each dot represents one tRNA. Two biologically independent samples are shown (R1, R2). **d**, Body weight changes after adoptive transfer of naive CD4<sup>+</sup> T cells into *Rag2*<sup>-/-</sup> host mice ( $n = 8$ ). Error bars represent mean  $\pm$  s.e.m. \*\*\*\* $P < 0.0001$ ; two-way ANOVA. **e**, Endoscopic colitis scores of the recipient mice 12 weeks posttransfer ( $n = 5$ ). Error bars represent mean  $\pm$  s.e.m. \*\*\* $P = 0.0002$ ; two-tailed, unpaired  $t$ -test. **f**, Representative endoscopic images of the colons of *Rag2*<sup>-/-</sup> mice receiving WT and *Trmt61a*-KO naive CD4<sup>+</sup> T cells 12 weeks posttransfer ( $n = 8$ ). Scale bars, 1 mm. **g**, Representative images of hematoxylin and eosin (H&E) and immunohistochemical (IHC) staining of the colons of *Rag2*<sup>-/-</sup> mice receiving WT or *Trmt61a*-KO naive CD4<sup>+</sup> T cells 12 weeks posttransfer ( $n = 8$ ). Scale bars, 250  $\mu$ m. **h**, Flow cytometric analysis of transferred CD4<sup>+</sup> T cell population in the spleen, peripheral lymph node (pLN) and mesenteric lymph node (mLN) of recipient mice 12 weeks posttransfer ( $n = 4$ ). Error bars represent mean  $\pm$  s.e.m. \*\* $P = 0.0011$ , \*\*\*\* $P < 0.0001$ ; two-tailed, unpaired  $t$ -test.

demonstrated a significant increase in bowel wall thickness, formation of crypt abscesses in severe cases and transmural infiltration of CD3<sup>+</sup> T cells (Fig. 2g). All these mice exhibited a ‘wasting syndrome’ 12 weeks after the transfer (Fig. 2d,e). By contrast,

mice that received *Trmt61a*-KO naive T cells continued to gain weight throughout the experiment, did not exhibit colitis upon endoscopy and had normal colon length compared with controls at 12 weeks after the transfer (Fig. 2d–g and Extended Data

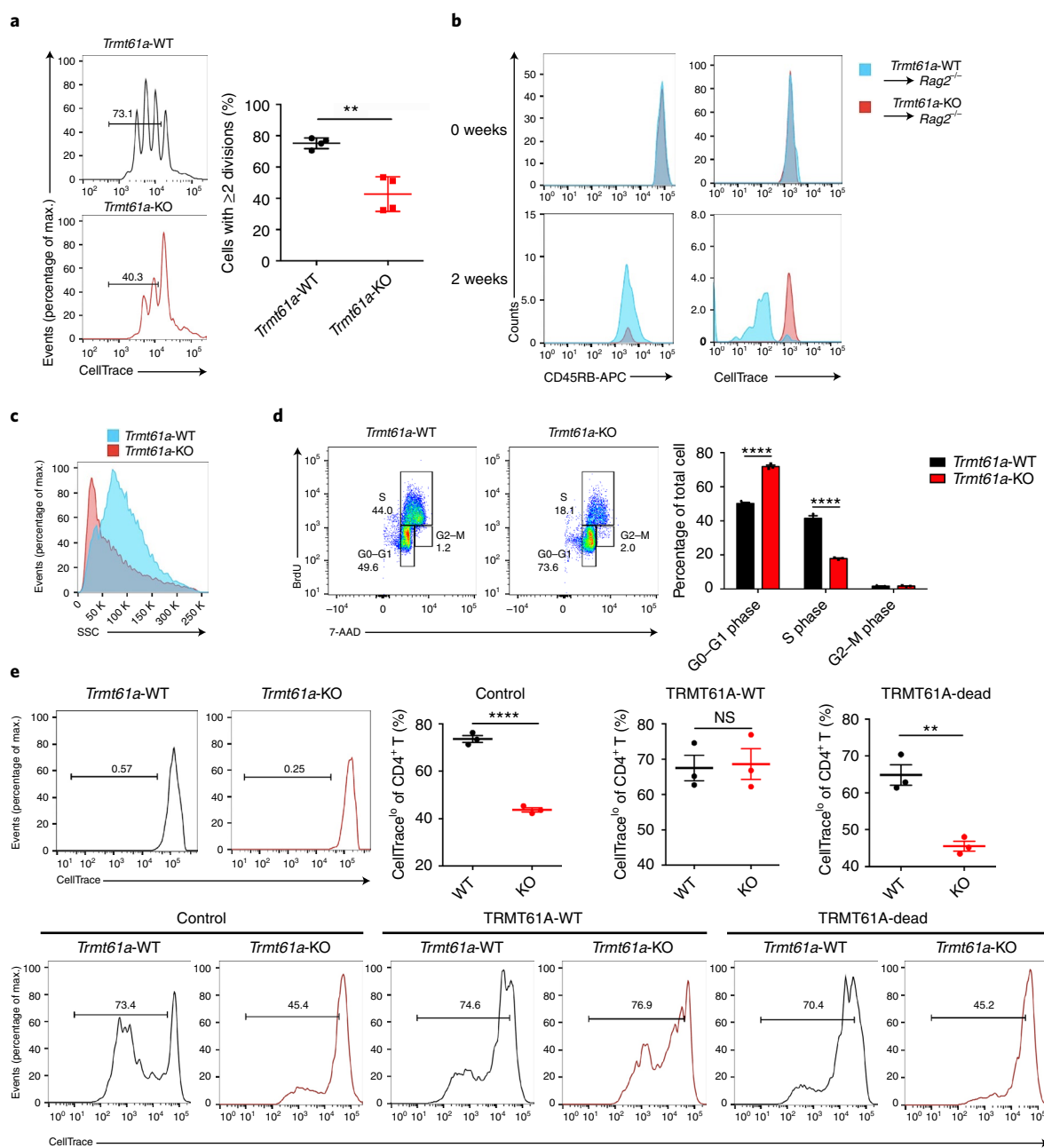


**Fig. 3 | TRMT61A-mediated tRNA-m<sup>1</sup>A58 promotes T cell proliferation.** **a**, Proliferation of WT naive CD4<sup>+</sup> T cells and *Trmt61a*-KO naive CD4<sup>+</sup> T cells in the presence of anti-CD3 and anti-CD28 antibodies, as measured by CellTrace dilution after 3 days. Error bars represent mean ± s.e.m., *n* = 4 biologically independent samples. \*\**P* = 0.0014; two-tailed, unpaired *t*-test. max., maximum. **b**, Naive CD4<sup>+</sup> T cells from *Trmt61a*-KO and WT mice were isolated and labeled with CellTrace and then transferred into *Rag2*<sup>-/-</sup> mice. At the time of transfer and 2 weeks later, CD45RB expression and CellTrace dilution in donor cells from the recipients' spleens were analyzed by flow cytometry. Representative data of four independent experiments are shown. **c**, Naive CD4<sup>+</sup> T cells were isolated from *Trmt61a*-KO and WT mice and activated with anti-CD3 and anti-CD28 antibodies for 48 h. Flow cytometry side-scatters (SSC) of activated CD4<sup>+</sup> T cells are shown. Representative data of three independent experiments are shown. **d**, Naive CD4<sup>+</sup> T cells were isolated from *Trmt61a*-KO and WT mice and activated with anti-CD3 and anti-CD28 antibodies for 48 h. Flow cytometry analysis of the cell cycle of activated CD4<sup>+</sup> T cells is shown. Error bars represent mean ± s.e.m., *n* = 3 biologically independent samples. \*\*\*\**P* < 0.0001; two-tailed, unpaired *t*-test. **e**, Retrovirus-mediated reexpression of TRMT61A-WT and catalytic-dead TRMT61A (TRMT61A-dead) in *Trmt61a*-KO and WT CD4<sup>+</sup> T cells. The cells were activated by anti-CD3 and anti-CD28 antibodies for 96 h. Flow cytometric analysis of CellTrace dilution is shown. Upper left: CellTrace dilution in unstimulated WT and *Trmt61a*-KO CD4<sup>+</sup> T cells; upper right: flow cytometric analysis of CellTrace dilution in different treatments; below: flow cytometry results showing CellTrace dilution in different treatment groups. Error bars represent mean ± s.e.m., *n* = 3 biologically independent samples. \*\**P* = 0.0034, \*\*\*\**P* < 0.0001; NS, nonsignificant; two-tailed, unpaired *t*-test.

Fig. 3c,d). Notably, WT naive T cells formed a stable cell population after 12 weeks of homeostatic expansion, but *Trmt61a*-KO naive T cells largely disappeared from the spleen and lymph nodes

of recipients (Fig. 2h). Taken together, these results demonstrate that TRMT61A is essential for the in vivo immune function of CD4<sup>+</sup> T cells.

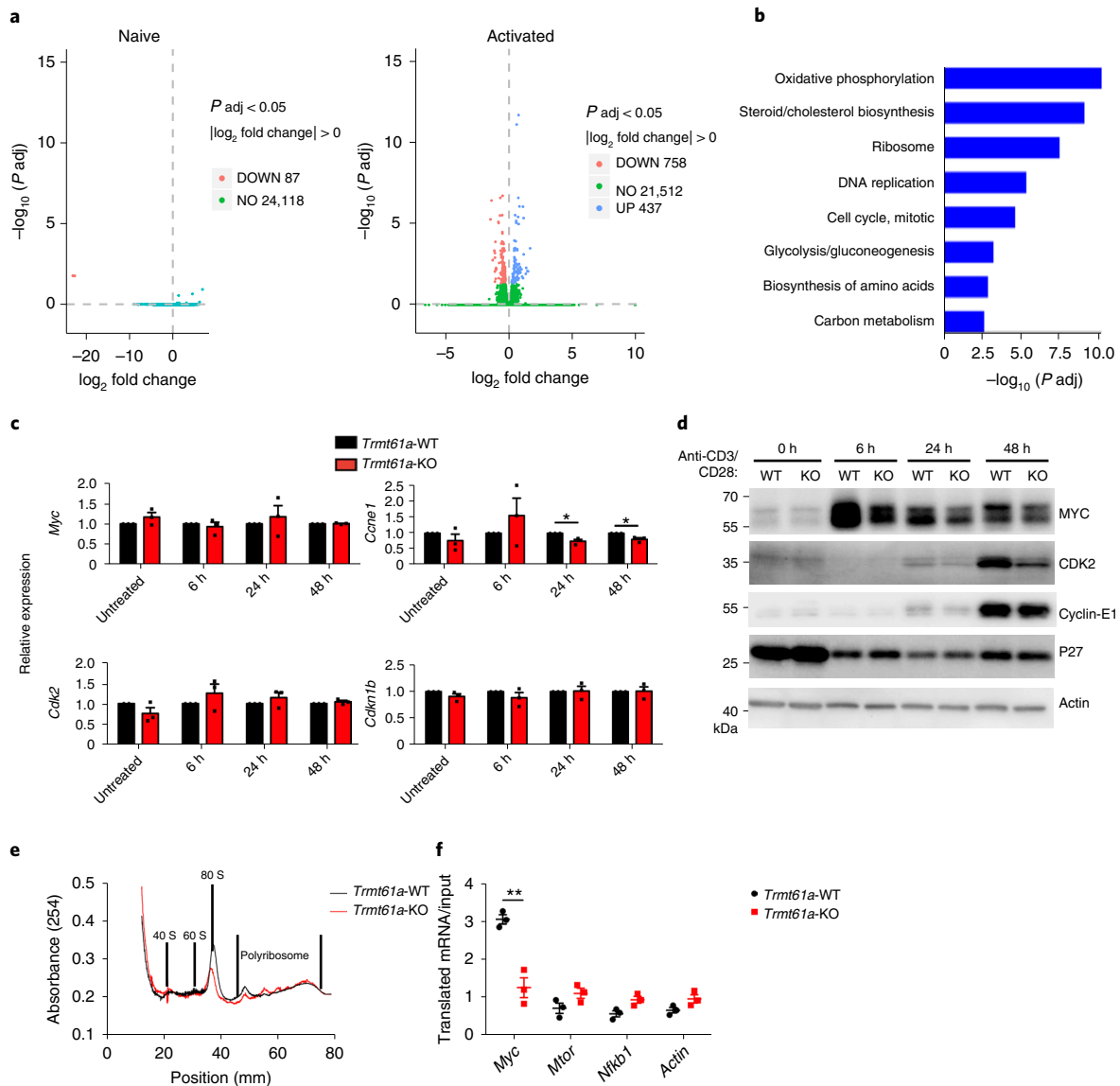


**Fig. 4 | tRNA-m<sup>1</sup>A58 is required for efficient *Myc* mRNA translation.** **a**, Volcano plots of RNA sequencing data of *Trmt61a*-KO naive CD4<sup>+</sup> T cells versus WT naive CD4<sup>+</sup> T cells (left) and *Trmt61a*-KO activated CD4<sup>+</sup> T cells versus WT activated CD4<sup>+</sup> T cells (right); the cells were activated by anti-CD3 and anti-CD28 antibodies for 48 h. Wald test (two-sided; adjustment method, Benjamini-Hochberg (BH)). **b**, KEGG enrichment analysis of the downregulated transcripts in *Trmt61a*-KO activated CD4<sup>+</sup> T cells versus WT activated CD4<sup>+</sup> T cells. Hypergeometric test (one-sided; adjustment method, BH). **c**, Real-time PCR measurements of levels of *Myc*, *Cdk2*, *Cdkn1b* and *Ccne1* mRNAs in *Trmt61a*-KO and WT naive CD4<sup>+</sup> T cells stimulated with anti-CD3 and anti-CD28 antibodies for 0, 6, 24 and 48 h. Error bars represent mean  $\pm$  s.e.m.,  $n = 3$  biologically independent samples from three independent experiments;  $*P = 0.0120$  (24 h),  $*P = 0.0164$  (48 h); two-tailed, unpaired *t*-test. **d**, Naive CD4<sup>+</sup> T cells obtained from the spleens of *Trmt61a*-KO and littermate control mice were stimulated for the indicated times with anti-CD3 and anti-CD28 antibodies. Levels of MYC, CDK2, P27 and cyclin E1 proteins were quantified by immunoblotting. Representative data of three independent experiments are shown. **e**, Representative trace of ribosome extract prepared from *Trmt61a*-KO and WT CD4<sup>+</sup> T cells in the presence of cycloheximide. The ribosomal extract was fractionated with a 5–50% sucrose gradient and analyzed using a pump syringe apparatus attached to an ultraviolet detector. Representative data of three independent experiments are shown. **f**, Ribosome occupancy of *Myc* and control mRNAs was measured by real-time PCR as the relative expression ratio (RER) of polyribosome mRNAs to the input mRNAs after sucrose gradient fractionation of polyribosomes. Error bars represent mean  $\pm$  s.e.m.,  $n = 3$  biologically independent samples.  $**P = 0.0032$ ; two-tailed, unpaired *t*-test.

### tRNA-m<sup>1</sup>A58 modification promotes T cell proliferation.

The reduction in the previously activated T cell population in *Trmt61a*-KO mice in a steady state and the attenuated immune function of *Trmt61a*-KO T cells in the adoptive transfer colitis model raised the possibility that TRMT61A deficiency might affect T cell activation, proliferation, apoptosis or differentiation<sup>34</sup>. To test these possibilities, we utilized in vitro T cell cultures by

stimulating purified primary naive CD4<sup>+</sup> T cells with anti-CD3 and anti-CD28 antibodies. We first measured the expression of early activation surface markers CD69 and CD44 by flow cytometry and observed that the activation of *Trmt61a*-KO T cells was normal and comparable with that of WT control cells (Extended Data Fig. 4a). Next, we examined the proliferative ability of the activated T cells using the CellTrace labeling and dilution assay and found

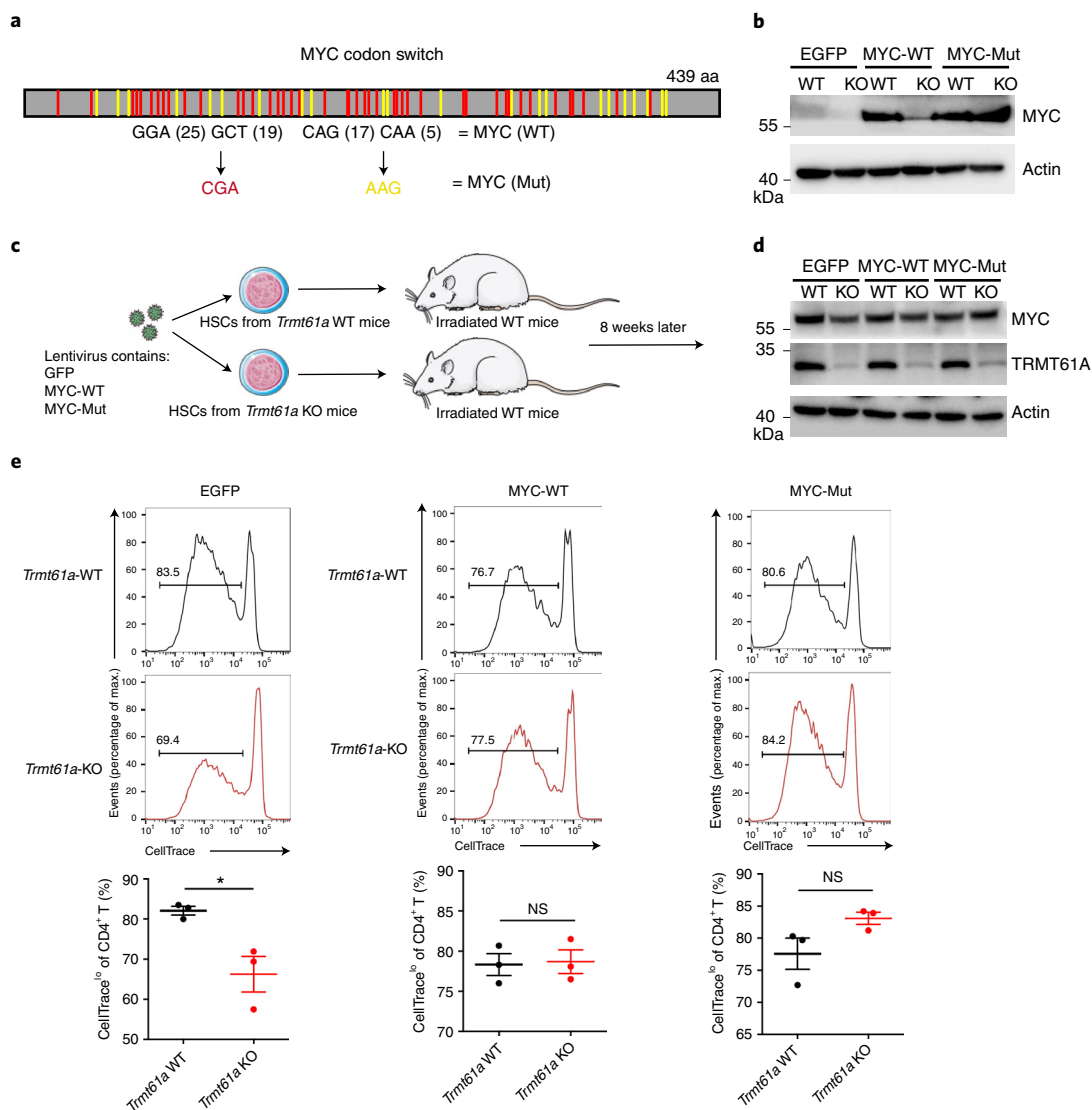


**Fig. 5 | MYC reduction contributes to proliferation defects.** **a**, Schematic diagram of the *Myc* codon-switch assay. aa, amino acid. **b**, Lentivirus-mediated expression of MYC-WT and MYC-mutant (MYC-Mut) in WT and *Trmt61a*-KO CD4<sup>+</sup> T cells. Protein levels of MYC were quantified by immunoblotting. Representative data of two independent experiments are shown. **c**, Schematic depicting HSC rescue assay. **d**, Protein levels of MYC in CD4<sup>+</sup> T cells from chimeric mice as quantified by immunoblotting. Cells were activated by anti-CD3 and anti-CD28 antibodies for 6 h. Representative data of three independent experiments are shown. **e**, Flow cytometric analysis of CellTrace dilution in CD4<sup>+</sup> T cells from chimeric mice. Cells were activated by anti-CD3 and anti-CD28 antibodies for 72 h. Error bars represent mean  $\pm$  s.e.m.,  $n=3$  biologically independent samples. \* $P=0.0257$ ; NS, nonsignificant; two-tailed, unpaired *t*-test.

that *Trmt61a*-deficient T cells proliferated much less than their WT counterparts (Fig. 3a and Extended Data Fig. 4b). We also assessed cell apoptosis by staining with Annexin V/7-aminoactinomycin D (7-AAD) but found that apoptosis was similar for WT and *Trmt61a*-KO CD4<sup>+</sup> T cells (Extended Data Fig. 4c). Finally, we used defined in vitro TCR-dependent T cell differentiation systems to investigate the involvement of *Trmt61a* in skewing T helper (T<sub>H</sub>) cell subset differentiation and found that *Trmt61a*-deficient naive CD4<sup>+</sup> T cells exhibited decreased subsets differentiation potential to become T<sub>H</sub>1, T<sub>H</sub>17 and in vitro-induced T<sub>reg</sub> (iT<sub>reg</sub>) cells, relative to WT naive CD4<sup>+</sup> T cells (Extended Data Fig. 4d–f). Together, these results suggest that TRMT61A promotes the proliferation and differentiation of CD4<sup>+</sup> T cells.

To investigate whether the proliferation and differentiation defects detected in vitro could also be observed in vivo, we used an adoptive transfer assay to measure T cell homeostatic activation and

proliferation ability. For this purpose, purified CD4<sup>+</sup>CD25<sup>−</sup>CD45RB<sup>hi</sup> naive T cells were labeled with CellTrace Violet and injected intravenously into *Rag2*<sup>−/−</sup> recipients. We analyzed the mice 2 weeks after transfer and found that *Trmt61a*-deficient cells failed to proliferate in *Rag2*<sup>−/−</sup> mice (Fig. 3b). These data further highlight the importance of TRMT61A in maintaining the proliferation ability of CD4<sup>+</sup> T cells after activation.

The rapid proliferation of T cells is associated with metabolic reprogramming and cell cycle progression upon activation. As expected, we found that granularity was remarkably reduced in *Trmt61a*-KO cells, as evidenced by the smaller side-scatter values obtained by flow cytometry (Fig. 3c). Furthermore, we performed a cell cycle analysis. In this assay, DNA synthesis was measured using BrdU, and the DNA amount was evaluated by 7-AAD staining. We found that in *Trmt61a*-KO T cells, the fraction of cells in S phase decreased whereas the fraction of cells in G0–G1 phase increased

strikingly in comparison with WT control cells (Fig. 3d). These data indicate that the progression of the cell cycle from G0–G1 phase to S phase is arrested in *Trmt61a*-KO CD4<sup>+</sup> T cells.

To establish whether the T cell proliferation defect resulting from TRMT61A deletion was indeed caused by the reduction in tRNA-m<sup>1</sup>A58 modification, we reintroduced the WT *Trmt61a* gene or m<sup>1</sup>A58 catalytic-dead *Trmt61a* gene into *Trmt61a*-KO CD4<sup>+</sup> T cells via retroviral transfection<sup>35</sup> (Extended Data Fig. 4g). The WT *Trmt61a*, but not m<sup>1</sup>A58 catalytic-dead *Trmt61a*, largely reversed the proliferation defect of *Trmt61a*-KO T cells in vitro, as evidenced by the results of the CellTrace labeling assay and cell number counting (Fig. 3e and Extended Data Fig. 4h). We also validated the rescue of m<sup>1</sup>A enzyme activity in vivo by performing similar retroviral transfection but adoptively transferring the transfected T cells into *Rag2*<sup>-/-</sup> recipient mice (Extended Data Fig. 4i).

Furthermore, we generated an additional *Cd4*<sup>Cre</sup> conditional KO mouse line for the TRMT6, an essential m<sup>1</sup>A catalytic partner for TRMT61A in the m<sup>1</sup>A ‘writer’ complex (Extended Data Fig. 5a–c). *Trmt6*-KO mice showed an identical phenotype to *Trmt61a*-KO mice (Extended Data Fig. 5d,e). Specifically, using the above methods, we found a similar proliferation defect of activated T cells isolated from *Trmt61a*-KO mice (Extended Data Fig. 5e). Thus, our data demonstrate that *Trmt61a*-deficiency-induced cell cycle arrest of activated CD4<sup>+</sup> T cells is due to the depletion of tRNA-m<sup>1</sup>A58 modification. Together, these findings show that tRNA-m<sup>1</sup>A58 modification is required for the robust proliferation of naive CD4<sup>+</sup> T cells after activation.

#### tRNA-m<sup>1</sup>A58 is required for efficient *Myc* mRNA translation.

T cell homeostasis and proliferation are mainly controlled by TCR signaling and the IL-2-signal transducer and activator of transcription 5 (STAT5) pathways at the very early stage<sup>36,37</sup>. To investigate the signaling pathways responsible for the observed T cell cycle arrest caused by *Trmt61a* deficiency, we first determined the effect of the loss of this gene on the TCR-induced signaling pathway and found that lack of TRMT61A did not affect the phosphorylation of the zeta chain of TCR-associated protein kinase 70 (ZAP70) or extracellular signal-regulated kinase (ERK) after TCR stimulation (Extended Data Fig. 6a). Given that IL-2 is an important cytokine for the proliferation of activated CD4<sup>+</sup> T cells<sup>36</sup>, we then examined the production of IL-2 by T cells and found that IL-2 expression at the protein level was similar in *Trmt61a*-deficient T cells and WT control cells (Extended Data Fig. 6b). Furthermore, immunoblotting showed that phosphorylation of STAT5 was comparable in *Trmt61a*-deficient CD4<sup>+</sup> T cells and their WT counterparts (Extended Data Fig. 6c), suggesting that activation of the Janus kinase (JAK)–STAT5 pathway by IL-2 remained normal after *Trmt61a* deletion. IL-7 is the critical factor driving homeostatic proliferation upon transfer of naive T cells to *Rag2*<sup>-/-</sup> KO mice<sup>38</sup>.

However, we did not detect a significant difference in IL-7 receptor–CD127 expression between WT and *Trmt61a*-KO naive T cells (Extended Data Fig. 6d), indicating that neither IL-2 nor IL-7 signaling was the cause of the failed T cell proliferation in *Trmt61a*-KO cells.

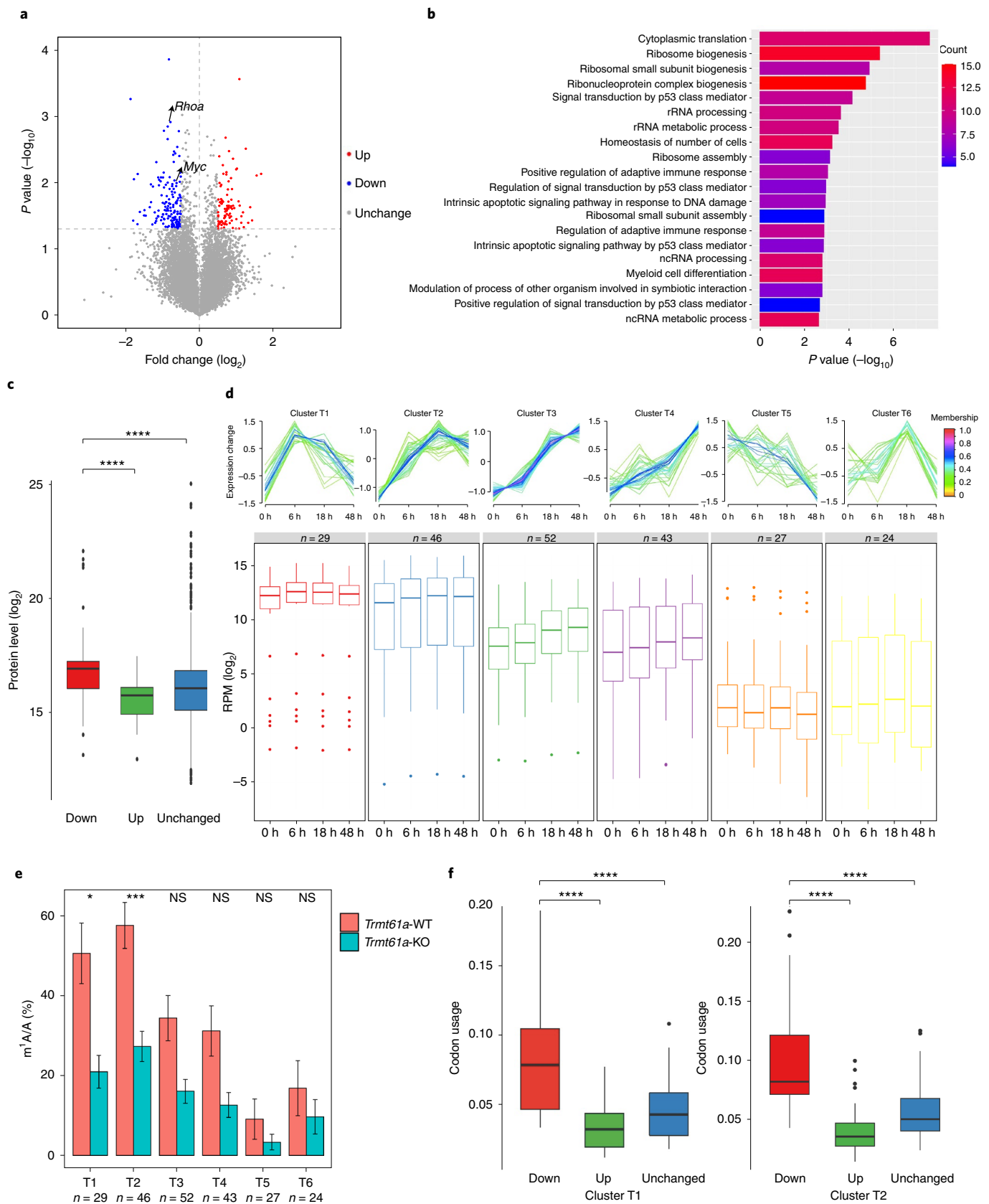
To systematically explore the molecular mechanism underlying the proliferation defect, we performed RNA sequencing analysis on the naive and in vitro activated T cells (48 h postactivation with anti-CD3 and anti-CD28 antibodies) from *Trmt61a*-KO mice and WT littermates. Consistent with the observed cell cycle arrest phenotypes, the genes that were significantly downregulated in the activated but not in the naive *Trmt61a*-KO cells were mostly involved in pathways related to cell metabolism and cell cycle (Fig. 4a,b). Previous studies have shown that the mammalian target of rapamycin complex 1 (mTORC1) is critical for cell metabolism, cell growth and cell cycle progression in the early stage of T cell activation<sup>34,39</sup>. Therefore, we first examined the activity of mTORC1 by stimulating the naive T cells with anti-CD3 and anti-CD28 antibodies for 3 or 6 h. We found that the phosphorylation levels of ribosomal protein S6 and eukaryotic translation initiation factor 4E binding protein 1 (4EBP1) were comparable between WT and *Trmt61a*-KO CD4<sup>+</sup> T cells (Extended Data Fig. 7a), thereby excluding the involvement of mTORC1-mediated signaling pathways in metabolic defects and cell cycle arrest in *Trmt61a*-KO cells.

MYC facilitates rapid metabolic reprogramming and cell proliferation of transformed cells<sup>1,40,41</sup>. Published proteomics data, as well as our time-course RNA sequencing data, has shown that MYC is rapidly induced upon T cell activation (Fig. 1d and Extended Data Fig. 7b)<sup>1</sup>. In addition, gene-set enrichment analysis of differentially expressed genes in activated CD4<sup>+</sup> T cells from *Trmt61a*-KO mice versus WT T cells showed that genes regulated by the MYC transcription factor were the most downregulated gene set (Extended Data Fig. 7c). Thus, we hypothesized that tRNA-m<sup>1</sup>A58 would directly promote efficient *Myc* mRNA translation, and that TRMT61A deficiency would lead to MYC reduction and cell cycle arrest at the exit phase from T cell quiescence. Accordingly, we measured MYC expression at both the protein and mRNA levels after incubating cells with anti-CD3 and anti-CD28 antibodies for 6, 24 and 48 h. Strikingly, we found that the level of MYC protein but not that of *Myc* mRNA was much lower in *Trmt61a*-deficient cells than in WT cells (Fig. 4c,d). Given the observed decrease in MYC protein levels, we next examined the known MYC-regulated targets. First, reducing the level of MYC protein indeed led to decreased protein expression of CDK2 and cyclin E (Fig. 4d), which are the key regulators of S phase<sup>42</sup>. Besides, MYC-dependent catabolism provides precursors for biosynthetic pathways during T cell activation<sup>41,43,44</sup>. Consistent with this notion, we observed that a significant fraction of genes downregulated at the transcript level in *Trmt61a*-KO CD4<sup>+</sup> T cells at

**Fig. 6 | Distinct codon usage leads to biased translation.** **a**, TE (FPKM in RiboTag-Seq divided by FPKM in input RNA sequencing) analysis of mRNA translation between *Trmt61a*-KO activated CD4<sup>+</sup> T cells (6 h) and WT control cells. *t*-test (two-sided, without adjustments). **b**, GO enrichment analysis of TE-down transcripts in activated *Trmt61a*-KO CD4<sup>+</sup> T cells versus activated WT CD4<sup>+</sup> T cells (6 h). Hypergeometric test (adjustment method, BH). ncRNA, noncoding RNA; rRNA, ribosomal RNA. **c**, Protein levels corresponding to TE-down genes ( $n=105$ ) and TE-up ( $n=32$ ) or unchanged genes ( $n=6589$ ) in the in vitro activated CD4<sup>+</sup> T cells (8 h). Data from the PRIDE database under accession number PXD004367. \*\*\*\* $P < 0.0001$ ; one-way ANOVA with Tukey’s multiple comparisons test. Boxes show median, upper and lower quartiles; whiskers show 1.5× IQR on either side; and points show outliers. **d**, Naive CD4<sup>+</sup> T cells were activated for 0, 3, 6 and 18 h. After tRNA sequencing, the dynamic expression changes of tRNAs in different groups were determined. Yellow or green lines correspond to genes with low membership value; red and purple lines correspond to genes with high membership value (top). RPM are shown as box plots (bottom) (boxes show median, upper and lower quartiles; whiskers show 1.5× IQR on either side; and the points show outliers). **e**, The corresponding m<sup>1</sup>A58 modification levels in different tRNA clusters are shown. Error bars represent mean ± s.e.m. \* $P=0.0170$ , \*\*\* $P=0.0009$ ; NS, nonsignificant; two-sided Wilcoxon signed-rank test. **f**, Analysis of codon usage of TE-down genes ( $n=117$ ) and TE-up ( $n=61$ ) or no changed genes ( $n=8569$ ). These codons were decoded by rapidly content-increased tRNAs within 6 h of T cell activation and with high sensitivity to *Trmt61a* deletion (clusters T1 ( $n=20$ ) and T2 ( $n=26$ )). Codon usage were calculated based on mRNA expression: codon usage =  $\sum \text{codon frequency in gene } i \times \text{mRNA expression of gene } i$ . \*\*\*\* $P < 0.0001$ ; one-way ANOVA with Tukey’s multiple comparisons test. Data are shown as box plots (boxes show median, upper and lower quartiles; whiskers show 1.5× IQR on either side; and the points show outliers).

48 h postactivation were involved in the biosynthesis of cholesterol and amino acids (Extended Data Fig. 7d). Taken together, these data show that *Trmt61a* deficiency mainly reduces MYC protein

levels during the early stage of T cell activation and consequently attenuates MYC-regulated cell cycling and metabolism during T cell proliferation.



Next, we sought to explore the mechanism whereby TRMT61A-mediated tRNA-m<sup>1</sup>A58 modification affects MYC protein levels. Previous studies have shown that MYC can be degraded by the ubiquitination degradation pathway<sup>45</sup>. Accordingly, we used the ubiquitination inhibitor MG132<sup>46</sup> and found that blocking the ubiquitination degradation pathway did not affect the reduction in MYC protein levels upon TRMT61A deletion (Extended Data Fig. 7e). This ruled out the possibility that the decrease in MYC protein levels could be caused by excessive protein degradation.

tRNA-m<sup>1</sup>A58 modification is required for efficient mRNA translation during initiation and elongation<sup>22</sup>. To establish whether *Myc* mRNA, through its codon content, requires tRNA-m<sup>1</sup>A58 modification during translation, we performed polyribosome real-time PCR experiments to quantify the ribosome occupancy of *Myc* mRNAs. Notably, we found a dramatic decrease in the accumulation of ribosomes on *Myc* mRNAs but not on control transcripts upon TRMT61A depletion (Fig. 4e,f). To determine whether MYC translation deficiency was due to mRNA translation initiation or elongation in *Trmt61a*-KO T cells, we analyzed the m<sup>1</sup>A58 levels and expression levels of initiator-methionine tRNA and found that neither was decreased in *Trmt61a*-KO cells (Extended Data Figs. 2c and 8a), suggesting that tRNA-m<sup>1</sup>A58 is more likely to regulate the translation elongation of *Myc* mRNA. Taken together, these results demonstrate that tRNA-m<sup>1</sup>A58 is essential for efficient *Myc* mRNA translation during T cell proliferation.

**MYC reduction contributes to the proliferation defect.** To further explore the potential molecular mechanisms of *Myc* translational enhancement by tRNA-m<sup>1</sup>A58 modification, we reanalyzed the tRNA-m<sup>1</sup>A sequencing data of WT versus *Trmt61a*-KO T cells to determine the magnitude of the reduction in m<sup>1</sup>A58 modification levels on each tRNA after TRMT61A deletion. We found that the m<sup>1</sup>A58 levels on most tRNAs were reduced to varying degrees after TRMT61A deletion, and the tRNAs decoding serine and leucine were among the most affected tRNAs (Extended Data Fig. 8b). Serine and leucine were also among the codons most frequently used by *Myc* mRNA; thus, we remodeled *Myc* cDNA such that the most abundant serine and leucine codons were replaced by their synonymous codons decoded by tRNAs least affected by TRMT61A deletion (Fig. 5a and Extended Data Fig. 8c). Accordingly, the TCC/AGC (serine) and TTG/CTG (leucine) codons were replaced by TCG (serine) and CTT (leucine) (Fig. 5a). Expression of this mutant *Myc* plasmid in WT and *Trmt61a*-deficient CD4<sup>+</sup> T cells was sufficient to rescue the defective expression of MYC in KO cells in vitro (Fig. 5b), confirming that tRNA-m<sup>1</sup>A58 modification directly regulates *Myc* mRNA translation through codon decoding.

To validate the contribution of MYC to the observed phenotypes of *Trmt61a*-deficient CD4<sup>+</sup> T cells, we overexpressed MYC protein via lentivirus in hematopoietic stem cells (HSCs) from WT and *Trmt61a*-KO mice and then transferred these HSCs into irradiated WT mice (Fig. 5c). Two months later, the transferred HSCs were assumed to reconstitute the irradiation-damaged immune systems of recipient mice. We isolated naive CD4<sup>+</sup> T cells from *Myc*-overexpressing WT and *Trmt61a*-KO HSC recipient mice and detected MYC protein levels and T cell proliferation after stimulation with anti-CD3 and anti-CD28 antibodies ex vivo. As expected, the mutant *Myc* plasmid was sufficient to rescue the defective protein expression of MYC in *Trmt61a*-KO cells, whereas the WT-*Myc* plasmid also slightly increased MYC protein levels in *Trmt61a*-KO cells (Fig. 5d). More importantly, both WT and mutant *Myc* plasmids mediated MYC protein expression to functionally restore the proliferation of *Trmt61a*-KO CD4<sup>+</sup> T cells (Fig. 5e), thereby confirming that the TRMT61A deficiency-induced proliferation defect was mainly MYC dependent. Taken together, these data demonstrate that efficient protein synthesis of MYC requires TRMT61A-mediated tRNA-m<sup>1</sup>A58 modification, which ensures

the quantity of MYC protein and enables activated T cells to rapidly undergo metabolic reprogramming, mitosis and proliferation.

**Distinct codon usage leads to biased translation.** Given the global reduction in tRNA-m<sup>1</sup>A58 after *Trmt61a* deletion, we speculated that the translation of other proteins besides MYC might also be affected. To accurately and systematically examine the translation efficiency (TE) of all mRNAs, we first bred *RiboTag*<sup>fllox/fllox</sup>*Cd4*<sup>Cre</sup> mice into *Trmt61a*<sup>fllox/fllox</sup> mice and then performed RiboTag RNA sequencing (RiboTag-Seq) with T cells 6h postactivation<sup>47</sup>. We found that m<sup>1</sup>A depletion reduced the TE of 114 genes, including *Myc* and *Rhoa* (Fig. 6a and Extended Data Fig. 9a,b). Gene ontology (GO) enrichment analysis of the TE-downregulated (TE-down) genes revealed that most of them were involved in translation and ribosome biogenesis (Fig. 6b), consistent with the essential role of TRMT6- and TRMT61A-mediated tRNA-m<sup>1</sup>A58 modification. We also selected *Cdk2*, as its protein level was decreased whereas its mRNA expression was unchanged in *Trmt61a*-KO T cells at 48h postactivation (Fig. 4c,d). Then, we performed a codon-switch assay and found that recoded mutant *Cdk2* and *Rhoa* could rescue the TE defects in *Trmt61a*-KO T cells, similar to the results for *Myc* genes (Fig. 5a,b and Extended Data Fig. 9c,d).

To identify whether the m<sup>1</sup>A58-regulated TE-down genes were required to encode key early proteins for T cell activation, we reanalyzed the published T cell time-point proteomics data (from the PRIDE database under accession number PXD004367)<sup>1</sup> and compared them with our RiboTag-Seq data. We found that TE-down genes from RiboTag-Seq were much more significantly enriched in a group of genes from the 8-h proteomics data compared with TE-up or TE-unchanged genes (Fig. 6c and Extended Data Fig. 9e). Furthermore, TE-down genes overlapped significantly with a group of continuously increasing proteins (38 out of 114 TE-down genes) but did not overlap with the other five clusters of genes in the time-point proteomics data (Extended Data Fig. 9f), indicating that this specific group of continuously increasing protein genes in the pre-cell-cycling stage was more sensitive to TRMT61A deletion. We also found that the TE-down group had a higher proportion of protein-up genes compared with the TE-up and TE-unchanged groups (Extended Data Fig. 9e). Together, these results provide evidence that TRMT6 and TRMT61A mediate the preferential promotion by tRNA-m<sup>1</sup>A58 of the TE of a group of specific genes essential for T cell proliferation.

As our RiboTag-Seq data showed that the translation of many genes remained unaffected, we next investigated why tRNA-m<sup>1</sup>A58 deficiency only affected certain specific genes. The composition and size of the tRNA pool directly control the decoding of genetic information. Thus, we first re-evaluated the expression dynamics of our time-point tRNA sequencing data. We observed that high-abundance T1 and T2 cluster tRNAs were markedly increased at the early stage (0 to 6h) after T cell exit from quiescence and activation, whereas the tRNAs of the other four clusters were less abundant, and their expression levels gradually increased or decreased over the time frame (Fig. 6d). Given that m<sup>1</sup>A58 directly controls the decoding efficiency of tRNAs, we hypothesized that the sequential usage of newly synthesized tRNAs led to the biased preferential translation of the abovementioned specific group of TE-down genes. To test our hypothesis, we first analyzed the effects of TRMT61A deficiency on m<sup>1</sup>A58 modification levels in different tRNA clusters and found that overall m<sup>1</sup>A58 modification levels were significantly decreased in cluster T1 and T2 tRNA species in *Trmt61a*-KO T cells, whereas the m<sup>1</sup>A58 modification of tRNAs in the other four clusters was not affected by TRMT61A deletion (Fig. 6e). Next, we analyzed and compared the cluster T1 and T2 tRNA codon utilization rates among different TE groups. We found that the TE-down mRNAs had significantly higher codon usage corresponding to the tRNAs in clusters T1 and T2 compared with the TE-up and TE-unchanged

mRNAs (Fig. 6f). Therefore, at the early stage after T cell activation, TRMT6 and TRMT61A preferentially modify a group of rapidly upregulated tRNA species that are preferentially required for protein synthesis of a group of essential genes for T cell cycling.

In view of these findings, we conclude that the TRMT61A-mediated tRNA-m<sup>1</sup>A58 modification is essential for the rapid upregulation of a group of tRNA species and the sufficient translation of a program of important genes, particularly *Myc* at the pre-cell-cycling stage upon T cell activation, thus serving as an epigenetic translational checkpoint to control T cell proliferation (Extended Data Fig. 10).

## Discussion

To protect the host from pathogens, CD4<sup>+</sup> T cells must be able to respond and reprogram themselves rapidly. This critical process is achieved by the timely synthesis of a large number of functional proteins. Here, we demonstrate that tRNA-m<sup>1</sup>A58 methylation serves as an epigenetic translational control and constitutes an important mechanism that enables the rapid synthesis of large numbers of functional proteins and drives activated T cells to enter mitosis and proliferate quickly. More specifically, by using genetic mouse models, high-throughput tRNA and RNA sequencing, transcriptome-wide m<sup>1</sup>A profiling and RiboTag-Seq, we found that: (1) translation is an active process of this genetic information processing in early T cell activation; (2) the expression of tRNAs and tRNA-m<sup>1</sup>A58 ‘writer’ proteins (TRMT6 and TRMT61A) is rapidly increased upon T cell activation in a very short time; and (3) as tRNA-m<sup>1</sup>A58 promotes translation, m<sup>1</sup>A58 in tRNA supports the rapid translation demands of activated T cells, particularly for proteins enriched with codons corresponding to tRNAs that need to be upregulated at the pre-cell-cycling stage of T cell activation. This emphasizes the importance of m<sup>1</sup>A58 modification as an important translational checkpoint to serve as a ‘gas pedal’ for T cell proliferation, in contrast to the mRNA-m<sup>6</sup>A modification and BTG1/2-mediated poly(A) tail length that we have previously described, which rather serve to ‘release the brake’ to exit the quiescent state for T cell activation<sup>7,38</sup>.

T cell activation and proliferation is a very complicated process, during which the cells need to synergize different molecular machineries to overcome various checkpoints. Here, we reveal that m<sup>1</sup>A is only one of the translational checkpoints, with more to be discovered. We have observed that tRNA expression is sequentially activated, and it will be very interesting to explore in the future how tRNA expression is regulated. As tRNAs carry the richest RNA modifications, how each tRNA species is modified by different types of modification is even more complicated. Consistent with a recent report by Rak et al.<sup>48</sup>, our results imply that increased expression of m<sup>1</sup>A ‘writers’ is required to maintain constant methylation levels, in proportion to the increased pool size of tRNAs during T cell activation. In addition, we did not observe m<sup>1</sup>A effects over the initiator-methionine tRNA; these modifications are more likely to affect translation elongation. This is consistent with reports by Saikia et al. and Wang et al.<sup>20,49</sup>

Hereby, our study establishes a model that reveals how an m<sup>1</sup>A-modified tRNA epigenetic translational modulator enables cellular control of global translation in proliferating T cells. This finding opens new avenues for investigation of the function of m<sup>1</sup>A in human health and disease. Activated T cells are among the most rapidly proliferating cells in the body. Given that an efficient immune response during infection or the maintenance of immune homeostasis depends on the ability of T cells to undergo rapid clonal expansion, our study may point to a previously unidentified therapeutic target to alleviate various T cell-related inflammatory diseases and a new strategy for cancer immunotherapy. Moreover, this type of epigenetic control will undoubtedly be involved in many similar biological scenarios.

## Online content

Any methods, additional references, Nature Research reporting summaries, source data, extended data, supplementary information, acknowledgements, peer review information; details of author contributions and competing interests; and statements of data and code availability are available at <https://doi.org/10.1038/s41590-022-01301-3>.

Received: 28 September 2021; Accepted: 4 August 2022;

Published online: 22 September 2022

## References

- Tan, H. et al. Integrative proteomics and phosphoproteomics profiling reveals dynamic signaling networks and bioenergetics pathways underlying T cell activation. *Immunity* **46**, 488–503 (2017).
- Saravia, J., Chapman, N. M. & Chi, H. Helper T cell differentiation. *Cell. Mol. Immunol.* **16**, 634–643 (2019).
- Buck, M. D., O’Sullivan, D. & Pearce, E. L. T cell metabolism drives immunity. *J. Exp. Med.* **212**, 1345–1360 (2015).
- Jones, R. G. & Thompson, C. B. Revving the engine: signal transduction fuels T cell activation. *Immunity* **27**, 173–178 (2007).
- Paillard, F., Sterkers, G. & Vaquero, C. Transcriptional and post-transcriptional regulation of TcR, CD4 and CD8 gene expression during activation of normal human T lymphocytes. *EMBO J.* **9**, 1867–1872 (1990).
- Taniuchi, I. & Ellmeier, W. Transcriptional and epigenetic regulation of CD4/CD8 lineage choice. *Adv. Immunol.* **110**, 71–110 (2011).
- Hwang, S. S. et al. mRNA destabilization by BTG1 and BTG2 maintains T cell quiescence. *Science* **367**, 1255–1260 (2020).
- Loo, T. T., Gao, Y. & Lazarevic, V. Transcriptional regulation of CD4<sup>+</sup> TH cells that mediate tissue inflammation. *J. Leukoc. Biol.* **104**, 1069–1085 (2018).
- Schimmel, P. The emerging complexity of the tRNA world: mammalian tRNAs beyond protein synthesis. *Nat. Rev. Mol. Cell Biol.* **19**, 45–58 (2018).
- Zaborske, J. M. et al. A nutrient-driven tRNA modification alters translational fidelity and genome-wide protein coding across an animal genus. *PLoS Biol.* **12**, e1002015 (2014).
- Oerum, S., Degut, C., Barraud, P. & Tisne, C. m1A post-transcriptional modification in tRNAs. *Biomolecules* **7**, 20 (2017).
- Song, J. et al. Differential roles of human PUS10 in miRNA processing and tRNA pseudouridylation. *Nat. Chem. Biol.* **16**, 160–169 (2020).
- Bjork, G. R., Wikstrom, P. M. & Bystrom, A. S. Prevention of translational frameshifting by the modified nucleoside 1-methylguanosine. *Science* **244**, 986–989 (1989).
- Pan, T. Modifications and functional genomics of human transfer RNA. *Cell Res.* **28**, 395–404 (2018).
- Chan, C. T. et al. A quantitative systems approach reveals dynamic control of tRNA modifications during cellular stress. *PLoS Genet.* **6**, e1001247 (2010).
- Cantara, W. A. et al. The RNA Modification Database, RNAMDB: 2011 update. *Nucleic Acids Res.* **39**, D195–D201 (2011).
- Boccalletto, P. et al. MODOMICS: a database of RNA modification pathways. 2017 update. *Nucleic Acids Res.* **46**, D303–D307 (2018).
- Li, X. et al. Transcriptome-wide mapping reveals reversible and dynamic N<sup>1</sup>-methyladenosine methylome. *Nat. Chem. Biol.* **12**, 311–316 (2016).
- Dominissini, D. et al. The dynamic N<sup>1</sup>-methyladenosine methylome in eukaryotic messenger RNA. *Nature* **530**, 441–446 (2016).
- Saikia, M., Fu, Y., Pavon-Eternod, M., He, C. & Pan, T. Genome-wide analysis of N<sup>1</sup>-methyl-adenosine modification in human tRNAs. *RNA* **16**, 1317–1327 (2010).
- Clark, W. C., Evans, M. E., Dominissini, D., Zheng, G. & Pan, T. tRNA base methylation identification and quantification via high-throughput sequencing. *RNA* **22**, 1771–1784 (2016).
- Liu, F. et al. ALKBH1-mediated tRNA demethylation regulates translation. *Cell* **167**, 816–828 (2016).
- Yamane, H. & Paul, W. E. Early signaling events that underlie fate decisions of naive CD4<sup>+</sup> T cells toward distinct T-helper cell subsets. *Immunol. Rev.* **252**, 12–23 (2013).
- Michalek, R. D. & Rathmell, J. C. The metabolic life and times of a T-cell. *Immunol. Rev.* **236**, 190–202 (2010).
- Hopper, A. K. Transfer RNA post-transcriptional processing, turnover, and subcellular dynamics in the yeast *Saccharomyces cerevisiae*. *Genetics* **194**, 43–67 (2013).
- Yoshihisa, T. Handling tRNA introns, archaean way and eukaryotic way. *Front. Genet.* **5**, 213 (2014).

27. Reinhold-Hurek, B. & Shub, D. A. Self-splicing introns in tRNA genes of widely divergent bacteria. *Nature* **357**, 173–176 (1992).
28. Lorenz, C., Lunse, C. E. & Morl, M. tRNA modifications: impact on structure and thermal adaptation. *Biomolecules* **7**, 35 (2017).
29. Kurachi, M. et al. The transcription factor BATF operates as an essential differentiation checkpoint in early effector CD8<sup>+</sup> T cells. *Nat. Immunol.* **15**, 373–383 (2014).
30. Ciofani, M. et al. A validated regulatory network for Th17 cell specification. *Cell* **151**, 289–303 (2012).
31. Chou, C. et al. c-Myc-induced transcription factor AP4 is required for host protection mediated by CD8<sup>+</sup> T cells. *Nat. Immunol.* **15**, 884–893 (2014).
32. Li, P. et al. STAT5-mediated chromatin interactions in superenhancers activate IL-2 highly inducible genes: functional dissection of the Il2ra gene locus. *Proc. Natl Acad. Sci. USA* **114**, 12111–12119 (2017).
33. Ostanin, D. V. et al. T cell transfer model of chronic colitis: concepts, considerations, and tricks of the trade. *Am. J. Physiol. Gastrointest. Liver Physiol.* **296**, G135–G146 (2009).
34. Gasper, D. J., Tejera, M. M. & Suresh, M. CD4 T-cell memory generation and maintenance. *Crit. Rev. Immunol.* **34**, 121–146 (2014).
35. Finer-Moore, J., Czudnochowski, N., O'Connell, J. D. 3rd, Wang, A. L. & Stroud, R. M. Crystal structure of the human tRNA<sup>m<sup>1</sup>A58</sup> methyltransferase-tRNA<sub>3<sup>lys</sup></sub> complex: refolding of substrate tRNA allows access to the methylation target. *J. Mol. Biol.* **427**, 3862–3876 (2015).
36. Popmihajlov, Z., Xu, D., Morgan, H., Milligan, Z. & Smith, K. A. Conditional IL-2 gene deletion: consequences for T cell proliferation. *Front Immunol.* **3**, 102 (2012).
37. Snook, J. P., Kim, C. & Williams, M. A. TCR signal strength controls the differentiation of CD4<sup>+</sup> effector and memory T cells. *Sci. Immunol.* **3**, eaas9103 (2018).
38. Li, H. B. et al. m<sup>6</sup>A mRNA methylation controls T cell homeostasis by targeting the IL-7/STAT5/SOCS pathways. *Nature* **548**, 338–342 (2017).
39. Frauwirth, K. A. et al. The CD28 signaling pathway regulates glucose metabolism. *Immunity* **16**, 769–777 (2002).
40. Marchingo, J. M., Sinclair, L. V., Howden, A. J. & Cantrell, D. A. Quantitative analysis of how Myc controls T cell proteomes and metabolic pathways during T cell activation. *eLife* **9**, e53725 (2020).
41. Wang, R. et al. The transcription factor Myc controls metabolic reprogramming upon T lymphocyte activation. *Immunity* **35**, 871–882 (2011).
42. Hydbring, P., Castell, A. & Larsson, L. G. MYC modulation around the CDK2/p27/SKP2 axis. *Genes* **8**, 174 (2017).
43. Yang, K. et al. T cell exit from quiescence and differentiation into Th2 cells depend on Raptor-mTORC1-mediated metabolic reprogramming. *Immunity* **39**, 1043–1056 (2013).
44. MacIver, N. J., Michalek, R. D. & Rathmell, J. C. Metabolic regulation of T lymphocytes. *Annu. Rev. Immunol.* **31**, 259–283 (2013).
45. Gupta, S., Seth, A. & Davis, R. J. Transactivation of gene expression by Myc is inhibited by mutation at the phosphorylation sites Thr-58 and Ser-62. *Proc. Natl Acad. Sci. USA* **90**, 3216–3220 (1993).
46. Lee, D. H. & Goldberg, A. L. Proteasome inhibitors: valuable new tools for cell biologists. *Trends Cell Biol.* **8**, 397–403 (1998).
47. McGlincy, N. J. & Ingolia, N. T. Transcriptome-wide measurement of translation by ribosome profiling. *Methods* **126**, 112–129 (2017).
48. Rak, R. et al. Dynamic changes in tRNA modifications and abundance during T cell activation. *Proc. Natl Acad. Sci. USA* **118**, e2106556118 (2021).
49. Wang, Y. et al. N<sup>1</sup>-methyladenosine methylation in tRNA drives liver tumourigenesis by regulating cholesterol metabolism. *Nat. Commun.* **12**, 6314 (2021).

**Publisher's note** Springer Nature remains neutral with regard to jurisdictional claims in published maps and institutional affiliations.

Springer Nature or its licensor holds exclusive rights to this article under a publishing agreement with the author(s) or other rightsholder(s); author self-archiving of the accepted manuscript version of this article is solely governed by the terms of such publishing agreement and applicable law.

© The Author(s), under exclusive licence to Springer Nature America, Inc. 2022

## Methods

**Mice.** *Trmt61a*-floxed mice were generated at Shanghai Biomodel Organism Science & Technology Development Co., Ltd., using a CRISPR-Cas9-based genome-editing system. The guide RNA and donor oligonucleotides used were as follows. For *Trmt61a* left-side *loxP*: 5'-TGCATGAACCATGTTGTCGG-3' and 5'-GACCAGCCTGATCTACATAGTGTCCAGCAGCCAAAGGCTATATAGGGAGGCTGTCTGAAAGACAAAATATAGCCCTGCATGAACCATGTTGTCGGTATGATGTTACACAAATTAGCTTTCTGTTCCCCATCTGTAAAGTGGTCATAAAATGTAAGGAAGAGGAT-3'; for *Trmt61a* right-side *loxP*: 5'-GTGCCCTATGAGGTCGGAGC-3' and 5'-TGGGAGCTAACCTGGGTTGGAGAAGAAAGAGGAGGAGGTGCCCTATGAGTCCGGA GCTGGGATTGCTTGTGCTGGCCAAAGGTGCTGACTGCTTTTTTTCTAGGCCAGCTG-3'.

*Trmt6*-floxed mice were generated at Cyagen Biosciences Inc. using a CRISPR-Cas9-based genome-editing system. The guide RNA and donor oligonucleotides used were as follows. For *Trmt6* left-side *loxP*: 5'-AAGAGA CTGAGATCTCCGATAGG-3' and 5'-GCTTGTCTTTGAAGTTGCTCTAA GAGACTGAGATCTCCGATAGGAAGGCTAATGCCTGACCCTTGGCAGT ACTTCATTAGTTTACATCCATTTCCAATGTGTAGATTGCCA-3'; for *Trmt6* right-side *loxP*: 5'-ATGCTAGAGAATTAGCCCAACGG-3' and 5'-CTT ATCTCAAAAAGGATCTTTCAGGATGCTAGAGAATTAGCCCAACGGTAA AAGTACTTGTCTCTGAGAAGATCCAGGTTTCAGTTCTGAACACC CACATGGTGCTCA-3'.

*Trmt6*<sup>fllox/fllox</sup> or *Trmt61a*<sup>fllox/fllox</sup> mice were crossed with *CD4*<sup>Cre</sup> mice to obtain conditional KO mice. *RiboTag*<sup>fllox/fllox</sup> (B6N.129 strain) mice as previously described<sup>50</sup> were obtained from Jackson Laboratories. Crossing these mice with *Cd4*<sup>Cre</sup> mice facilitates the inclusion of an HA-epitope tag on the ribosomal protein RPL22 in all CD4-expressing cells. *Trmt6*<sup>fllox/fllox</sup> or *Cd4*<sup>Cre</sup> mice was used as WT littermate controls for *Trmt6*<sup>fllox/fllox</sup>*Cd4*<sup>Cre</sup> mice, *Trmt61a*<sup>fllox/fllox</sup> or *Cd4*<sup>Cre</sup> mice was used as WT littermate controls for *Trmt61a*<sup>fllox/fllox</sup>*Cd4*<sup>Cre</sup> mice. For all experiments, 6–12-week-old sex-matched mice were used, unless otherwise indicated. All the mice were bred and maintained under specific-pathogen-free conditions at the animal facility of Shanghai Biomodel Organism Science & Technology Development Co., Ltd. Animal procedures were approved by the Institutional Animal Care and Use Committee of Shanghai Jiao Tong University School of Medicine.

**Tissue preparation and flow cytometry.** Thymus, spleen, and peripheral and mesenteric lymph nodes were collected and pressed through a 200-gauge mesh. Spleen cells were prepared by lysing erythrocytes with red blood cell lysis buffer (Thermo Fisher Scientific). Monoclonal antibodies against CD3 (clone 145-2C11), CD4 (clones RM4-5, RM4-4, GK1.5), CD8 (clone 53-6.7), CD25 (clone 3C7), CD44 (clone IM7), CD62L (clone MEL-14), CD45 (clone 30-F11), CD45RB (clone C363-16A), CD62L (clone MEL-14), CD69 (clone H1.2F3), CD127 (clone A7R34), FOXP3 (clone MF-14), IFN- $\gamma$  (clone XMGL.2), IL-2 (clone JES7-5H4), IL-17A (clone TC11-18H10.1), Ki67 (clone 16A8) and TCR- $\beta$  (clone H57-597) were purchased from BioLegend. FOXP3 (clone FJK-16s) was purchased from Thermo Fisher Scientific. The cells were stained with antibodies (1:200) at 4°C for 30 min. For intracellular cytokine staining, cells were stimulated with phorbol myristate acetate phorbol 12-myristate 13-acetate (50 ng ml<sup>-1</sup>; Sigma), ionomycin (1  $\mu$ g ml<sup>-1</sup>; Sigma) and GolgiPlug (1  $\mu$ l ml<sup>-1</sup>; BD Biosciences) for 4 h. After surface antibody staining, cells were fixed and permeabilized with a Fixation/Permeabilization Solution Kit (BD Biosciences), followed by staining with antibodies against intracellular molecules. For intracellular transcription factor staining, cells were fixed and permeabilized using a FOXP3/Transcription Factor Buffer Set (BioLegend). Data were collected with a BD Fortessa X20 (BD Biosciences) and analyzed in FlowJo.

**T cell isolation and stimulation.** Naive CD4<sup>+</sup> or total CD4<sup>+</sup> T cells were purified by using an EasySep Mouse Naive CD4<sup>+</sup> T or CD4<sup>+</sup> T Cell Isolation Kit (STEMCELL Technologies) according to the respective instructions. The purified T cells were stimulated with plate-bound anti-CD3 (5  $\mu$ g ml<sup>-1</sup>) and anti-CD28 (2  $\mu$ g ml<sup>-1</sup>) in replicate wells of 96-well plates. Naive CD4<sup>+</sup> T cells labeled with CellTrace (Thermo Fisher Scientific, cat. no. C34557) were stimulated with antibodies against CD3 and CD28 for 72 h. The proliferation of the cells was determined and analyzed by CellTrace dilution. Total CD4<sup>+</sup> T cells were stimulated with antibodies against CD3 and CD28 for 16 h, and an APC Annexin V Apoptosis Detection Kit with 7-AAD (BioLegend) was used to analyze cell apoptosis. Naive CD4<sup>+</sup> T cells were stimulated for 48 h. BrdU/7-AAD cell cycle staining was performed according to the instructions for the FITC BrdU Flow Kit (BD Biosciences).

**T cell ex vivo differentiation.** Naive CD4<sup>+</sup> T cells were purified and polarized using a CellXVivo Mouse Th1 Cell Differentiation Kit (R&D Systems), CellXVivo Mouse Th17 Cell Differentiation Kit (R&D Systems) and CellXVivo Mouse Treg Cell Differentiation Kit (R&D Systems) according to the instructions. After culturing for 5 days, the cells were analyzed using a flow cytometer.

**Real-time PCR.** Total RNA was isolated from CD4<sup>+</sup> T cells with TRIzol reagent (Invitrogen) according to the manufacturer's instructions and then

reverse-transcribed with TransScript All-in-One First-Strand cDNA Synthesis SuperMix (TransGen Biotech, cat. no. AT341-02). iTaq Universal SYBR Green Supermix (Bio-Rad, cat. no. 1725124) was used for real-time PCR. *L32* was set as an internal control to calculate relative amounts of mRNA. The primer sequences used for real-time PCR were as follows:

*L32* (forward, 5'-ATGGCTCCTTCGTTGCTGC-3'; reverse, 5'-CTGGACGGCTAATGCTGGT-3'),  
*Actb* (forward, 5'-GGCTGTATCCCTCCATCG-3'; reverse, 5'-CCAGTTGGTAAACAATGCCATGT-3'),  
*Trmt61a* (forward, 5'-CGCACGCAGATCCTCTACTC-3'; reverse, 5'-GGAACCTACTGTGTGTAGGTGG-3'),  
*Trmt6* (forward, 5'-CATCGGCCATAGTTACGGCTC-3'; reverse, 5'-TCTGTCTTGTACGGAATGTTG-3'),  
*Mtor* (forward, 5'-ACCGGCACACATTTGAAGAAG-3'; reverse, 5'-CTCGTTGAGGATCAGCAAGG-3'),  
*Nfkb1* (forward, 5'-ATGGCAGACGATGATCCCTAC-3'; reverse, 5'-TGTTGACAGTGGTATTTCTGGT-3'),  
*Cdk2* (forward, 5'-GCGACCTCCCAATATCG-3'; reverse, 5'-GTCTGATCTTTCCTCAACTCT-3'),  
*Cdkn1b* (forward, 5'-TCAAACGTGAGAGTGTCTAACG-3'; reverse, 5'-CCGGGCCGAAGAGATTCTG-3'),  
*Ccne1* (forward, 5'-GTGGCTCCGACCTTTCAGTC-3'; reverse, 5'-CACAGCTTGTCAATCTTGGCA-3'),  
*Myc* (forward, 5'-ATGCCCTCAACGTGAACCTTC-3'; reverse, 5'-CGCAACATAGGATGGAGAGCA-3').

**Immunoblotting.** Total protein from CD4<sup>+</sup> T cells was extracted with radioimmunoprecipitation assay buffer (Beyotime, P0013E) supplemented with protease and phosphatase inhibitor cocktail (Thermo Fisher Scientific, cat. no. 78443). Antibodies against TRMT61A (Thermo Fisher Scientific, cat. no. PA5-76553), TRMT6 (Proteintech, cat. no. 16727-1-AP), MYC (Proteintech, cat. no. 10828-1-AP), cyclin E1 (Proteintech, cat. no. 11554-1-AP), P27 (Proteintech, cat. no. 25614-1-AP), p-ZAP70 (Cell Signaling Technology, cat. no. 2717), ZAP70 (Cell Signaling Technology, cat. no. 3165), p-ERK (Cell Signaling Technology, cat. no. 4370), ERK (Cell Signaling Technology, cat. no. 4695), p-STAT5 (Cell Signaling Technology, cat. no. 4322), STAT5 (Cell Signaling Technology, cat. no. 94205), RHOA (Cell Signaling Technology, cat. no. 2117), p-4EBP1 (Cell Signaling Technology, cat. no. 2855), p-S6 (Cell Signaling Technology, cat. no. 4858), ACTIN (Cell Signaling Technology, cat. no. 3700), CDK2 (Abcam, cat. no. ab32147), c-JUN (CST, cat. no. 9165) and FOSL2 (Abcam, cat. no. ab216838) were diluted in 5% non-fat milk buffer at a concentration of 1:2000 and incubated at 4°C overnight. After washing three times with phosphate-buffered saline (PBS) containing 0.1% Tween-20 buffer, horseradish peroxidase (HRP)-conjugated secondary antibody (anti-rabbit IgG, HRP-linked antibody, Cell Signaling Technology, cat. no. 7074; 1:10000; anti-mouse IgG, HRP-linked antibody, Biodragon, cat. no. BF03001; 1:10000) was added to the membranes, followed by incubation at room temperature for 1 h. The signal was detected by enhanced chemiluminescence with Pico ECL using ChemiDoc MP (Bio-Rad).  $\beta$ -ACTIN (Cell Signaling Technology, cat. no. 3700S) was used as an internal control.

**RNA sequencing of CD4<sup>+</sup> T cells from WT and *Trmt61a*<sup>fllox/fllox</sup>*Cd4*<sup>Cre</sup> mice.** The purified CD4<sup>+</sup> naive T cells were stimulated with plate-bound anti-CD3 (5  $\mu$ g ml<sup>-1</sup>) and anti-CD28 (2  $\mu$ g ml<sup>-1</sup>) in replicate wells of a 96-well plate. A total amount of 3  $\mu$ g RNA per sample was used as input material for the RNA sample preparations. Sequencing libraries were generated using a NEBNextUltra RNA Library Prep Kit for Illumina (NEB) following the manufacturer's recommendations, and index codes were added to attribute sequences for each sample. The clustering of the index-coded samples was performed on a cBot Cluster Generation System using TruSeq PE Cluster Kit v3-cBot-HS (Illumina) according to the manufacturer's instructions. After cluster generation, the library preparations were sequenced on an Illumina HiSeq platform, and 125-bp (base pair) to 150-bp paired-end reads were generated.

**RNA sequencing of CD4<sup>+</sup> T cell activation for different time points.** The purified T cells from each mouse were stimulated with plate-bound anti-CD3 (5  $\mu$ g/ml) and anti-CD28 (2  $\mu$ g/ml) for 0, 3, 6 and 18 hours. Total RNA was extracted based on the manufacturer's protocol by using TRIzol reagent (Invitrogen). RNA libraries were prepared using NEBNextUltra II Directional RNA Library Prep Kit for Illumina (NEB) based on the manufacturer's instructions. Illumina HiSeq X Ten platform (150-bp paired-end reads) was adopted by OE Biotech Co. Ltd. to sequence the libraries.

**RNA sequencing analysis.** Raw data (raw reads) in fastq format were first processed through fastp (v.0.17.0) with parameters '-qualified\_quality\_phred 5-unqualified\_percent\_limit 50-n\_base\_limit 15-min\_trim\_length 10-overlap\_len\_require 30-overlap\_diff\_limit 1-overlap\_diff\_percent\_limit 10-length\_required 150-length\_limit 150-trim\_poly\_g'. In this step, clean data (clean reads) were obtained by removing reads containing adapter or poly-N sequences and low-quality reads from raw data. Reference genome and gene model annotation

files were downloaded from the genome website ([http://ftp.ensembl.org/pub/release-94/gtf/mus\\_musculus/Mus\\_musculus.GRCm38.94.gtf.gz](http://ftp.ensembl.org/pub/release-94/gtf/mus_musculus/Mus_musculus.GRCm38.94.gtf.gz) and [http://ftp.ensembl.org/pub/release-94/fasta/mus\\_musculus/dna/Mus\\_musculus.GRCm38.dna.primary\\_assembly.fasta](http://ftp.ensembl.org/pub/release-94/fasta/mus_musculus/dna/Mus_musculus.GRCm38.dna.primary_assembly.fasta)). The index of the reference genome was built and paired-end clean reads were aligned to the reference genome using HISAT2 v.2.0.5; featureCounts v.1.5.0-p3 was used to count the numbers of reads mapped to each gene. The FPKM (fragments per kilobase of transcript per million mapped reads) value of each gene was calculated based on the length of the gene and the count of reads mapped to this gene. Differential expression analysis of two conditions or groups was performed using the DESeq2 R package (v.1.16.1). DESeq2 provides statistical routines for determining differential expression in digital gene expression data using a model based on the negative binomial distribution. The resulting *P* values were adjusted using Benjamini and Hochberg's approach for controlling the false discovery rate. Genes with an adjusted *P* value <0.05 identified by DESeq2 were assigned as differentially expressed. GO enrichment analysis of differentially expressed genes was performed with the clusterProfiler R package<sup>51</sup>, and gene length bias was corrected. GO terms with corrected *P* value less than 0.05 were considered to be significantly enriched for differentially expressed genes. We used the clusterProfiler R package to test the statistical enrichment of differentially expressed genes in KEGG pathways.

#### CD45RB<sup>hi</sup> adoptive transfer colitis, endoscopic and histologic analysis.

Purified CD4<sup>+</sup>CD25<sup>-</sup>CD45RB<sup>hi</sup> naive T cells from WT and *Trmt61a*<sup>lox/lox</sup>*Cd4*<sup>Cre</sup> mice were sorted by fluorescence-activated cell sorting (FACS), washed twice with PBS and counted, and 0.5 million cells were intravenously injected into each *Rag2*<sup>-/-</sup> recipient mouse. The recipient mice were monitored and weighed each week. After 8 weeks, colon colitis was visualized using an endoscope system (Cold Light Fountain XENON 175 SCB and IMAGE1 S D3-LINK, Karl Storz). Briefly, the colitis score was evaluated by considering the consistency of stools, the granularity of the mucosal surface, the translucency of the colon, fibrin deposits and vascularization of the mucosa (0–3 points for each parameter).

**Histological analysis.** After the colitis model was established, mice were sacrificed and their colons were fixed with 10% neutral-buffered formalin and embedded in paraffin. Serial paraffin sections (5 μm) were stained with hematoxylin and eosin and anti-CD3 immunohistochemical Ab to assess tissue inflammation and T cell infiltration.

**T cell homeostatic proliferation in vivo.** For T cell homeostatic proliferation in vivo, we labeled FACS-purified CD4<sup>+</sup>CD25<sup>-</sup>CD45RB<sup>hi</sup> naive cells with CellTrace before intravenous injection. We then intravenously injected 1 million cells into each *Rag2*<sup>-/-</sup> recipient mouse. We analyzed the CD45RB expression and CellTrace dilution in donor cells from the recipients' spleens at 2 weeks after injection by flow cytometry.

#### Quantification of m<sup>1</sup>A levels by liquid chromatography with mass spectrometry.

Isolated RNA (100 ng) was digested into nucleosides by 0.5 U nuclease P1 (Sigma) in 20 μl buffer containing 10 mM ammonium acetate, pH 5.3, at 42 °C for 6 h, followed by addition of 2.5 μl 0.5 M MES buffer, pH 6.5, and 0.5 μl shrimp alkaline phosphatase (NEB). The mixture was incubated at 37 °C for another 6 h and diluted to 100 μl. Then, 5 μl of the solution was subjected to liquid chromatography with mass spectrometry. The nucleosides were separated by ultra-performance liquid chromatography with a C18 column and then detected using a triple-quadrupole mass spectrometer (AB SCIEX QTRAP 5500) in the positive-ion multiple reaction monitoring mode. The mass transitions of *m/z* 282.0 to 150.1 (*m*<sup>1</sup>A), *m/z* 282.0 to 150.1 (*m*<sup>2</sup>A), and *m/z* 268.0 to 136.0 (A) were monitored and recorded. Concentrations of nucleosides in RNA samples were deduced by fitting the signal intensities to the standard curves.

**Quantitative tRNA m<sup>1</sup>A-seq.** The small RNA fraction (200 ng; <200 nucleotides (nt), mainly composed of mature tRNA) was purified from total RNA using a MEGAclear Kit (Thermo Fisher Scientific). Purified small RNA was deacetylated by incubation in 0.1 M Tris-HCl, pH 9, at 37 °C for 45 min. Half of the deacetylated small RNA fraction was subjected to demethylation treatment by an ALKB in vivo reaction. The total 20 μl mixture for ALKB-mediated demethylation included 0.8 pmol purified ALKB protein, 50 mM 2-(*N*-morpholino) ethanesulfonic acid (MES, pH 6.5), 300 μM 2-ketoglutarate, 283 μM (NH<sub>4</sub>)<sub>2</sub>Fe(SO<sub>4</sub>)<sub>2</sub>·6H<sub>2</sub>O, 2 mM L-ascorbic acid and 0.4 U μl<sup>-1</sup> RNase inhibitor. After 2 h incubation at 37 °C, 5 mM EDTA was added to quench the demethylation reaction, and the demethylated RNA was purified using phenol-chloroform extraction and subsequent ethanol precipitation. The demethylated and untreated RNA were together sent for library construction as previously described. Specifically, the 3' ends of RNA samples were first dephosphorylated using PNK with 37 °C incubation for 1 h and then heat-inactivated at 65 °C for 20 min, followed by ethanol precipitation. A 3' RNA linker (5'-rAPP-AGATCGGAAGAGCGGTGTG-3SpC3) was ligated to the dephosphorylated RNA using T4 RNA ligase 2, truncated KQ (NEB) at 25 °C for 2 h. The excess RNA linker was digested by adding 1 μl 5' deadenylase (NEB) with 30 °C incubation for 1 h, followed by addition of 1 μl RclJf (NEB) with 37 °C incubation for 1 h. The reaction was then heat-inactivated at 70 °C for 20 min, and

the 3' end ligated RNA was purified by ethanol precipitation. Then, 10 μl H<sub>2</sub>O was used to dissolve the recovered RNA pellet, and 1 μl reverse transcription (RT) primer (ACACGAGCTCTCCGATCT; 2 μM) was added. The RNA-primer mixture was denatured by incubation for 2 min at 80 °C and then immediately chilled on ice. RT reaction buffer was prepared according to the following formula: 50 mM Tris-HCl (pH 8.3), 75 mM KCl, 3 mM MgCl<sub>2</sub>, 1 mM dNTPs, 5 mM DTT, 1 U μl<sup>-1</sup> RNase inhibitor and 1 μl TGIRT (InGex). The reaction buffer was well mixed and then added to the denatured RNA-primer mixture, followed by incubation at 57 °C for 2 h for the RT reaction. Exonuclease I (NEB; 1 μl) was added, followed by incubation at 37 °C for 30 min to digest the excess RT primer. The resulting cDNA was purified with silane beads (Invitrogen) and then subjected to 5' adapter ligation (5Phos-NNNNNNNNNAGATCGGAAGAGCACACGTCTG-3SpC3) by a 25 °C overnight reaction after adding 1 μl high-concentration T4 RNA ligase 1 (NEB). The resulting cDNA was again purified with silane beads. PCR amplification was carried out using the following primers: 5'-AATGATACGGGACCACCGAGATCTACACTCTTTCCCTA CACGAGCTCTCCGATCT-3', 5'-CAAGCAGAAGACGGCATAACGAGA TXXXXXXGTGACTGGAGTTCAGACGTGTGCTCTCCGATC-3' (where XXXXXX represents the index sequence). The library was purified using 8% Tris-Borate-EDTA gel and then subjected to sequencing on an Illumina HiSeq X10 platform (PE 150).

**tRNA m<sup>1</sup>A-seq analysis.** Raw read adapter sequences were trimmed with trim\_galore v.0.6.5; the minimum quality threshold was set to 20, and the minimum length required for reads after trimming was 30 nt. The remaining reads were further processed by removing the first 10 nt of random barcodes at the 5' end. Processed reads were mapped to the mouse tRNA reference (<http://gtradb.ucsc.edu/genomes/eukaryota/Mmus10/Mmus10-seq.html>) using BWA-MEM with default parameters. Reads mapped to identical positions of the reference were considered to be PCR duplications if their 10-nt random barcodes were the same, and only one of these reads was kept. SAM and BAM files were processed with the help of samtools. For identification of m<sup>1</sup>A sites, the mismatch rate of each nucleotide in the reference sequences was calculated for both demethylase untreated (-) and demethylase-treated (+) samples. m<sup>1</sup>A sites were defined using the following criteria: (1) tRNA coverage >200; (2) fold change of mismatch rates in (-) demethylase relative to mismatch rates in (+) demethylase ≥3; (3) difference between mismatch rates of (-) demethylase and mismatch rates of (+) demethylase >10%; (4) corresponding reference base is A. For identification of m<sup>3</sup>C and m<sup>3</sup>G sites, criteria 1, 2 and 3 were the same as for the m<sup>1</sup>A cut-off, and the corresponding reference bases were C and G, respectively.

**tRNA sequencing analysis.** Raw read adapter sequences were trimmed with trim\_galore v.0.6.5, and the minimum quality threshold was set to 20. Processed reads were mapped to the mouse tRNA reference using BWA-MEM with default parameters. Reads per million mapped reads were calculated by manual scripts. tRNA groups were clustered with ComplexHeatmap<sup>52</sup>, using *k*-means clustering (parameters: row\_km = 5, row\_km\_repeats = 800).

**TRMT61A-KO rescue.** Retroviral transduction was performed by transfecting HEK293T cells with an MG-guide-retrovirus (replace EGFP) plasmid encoding WT or D181A-mutant TRMT61A along with packaging plasmids (the sequence was analyzed using SnapGene v.4.1.6). Purified *Trmt61a*-deficient naive CD4<sup>+</sup> T cells were activated in a 48-well plate for 48 h and then infected with the packaged retrovirus in the presence of 8 mg ml<sup>-1</sup> polybrene and CellTrace by spinning at 1000g for 90 mins. Forty-eight hours after retrovirus infection at 37 °C, the proliferation of the cells was determined and analyzed by CellTrace dilution. Cell numbers were counted by flow cytometry using Precision Count Beads (BioLegend, cat. no. 424902). For in vivo assays, cells were labeled with CellTrace and transferred into *Rag2*<sup>-/-</sup> recipient mice by intravenous injection (one million cells per mouse). Two weeks after transfer, cells from spleens, periphery lymph nodes, and mesenteric lymph nodes were analyzed by flow cytometry.

**Codon-switch assay.** The coding DNA sequences of WT-*Myc*, mut-*Myc*, WT-*Cdk2*, mut-*Cdk2*, WT-*Rhoa* and mut-*Rhoa* were constructed into a pLVX-IRES-ZsGreen plasmid. Lentivirus was produced in 293T cells using the standard protocols. Transfection was performed using X-tremeGENE HP DNA Transfection Reagent (Roche). Purified WT and *Trmt61a*-deficient naive CD4<sup>+</sup> T cells were activated in a 48-well plate for 48 h and then infected with the packaged lentivirus in the presence of 8 mg ml<sup>-1</sup> polybrene by spinning at 1000g for 90 min. Cells were collected for immunoblot analysis 48 h after infection at 37 °C.

**RiboTag RNA sequencing.** Ten million naive CD4<sup>+</sup> T cells were isolated from WT (*RiboTag*<sup>lox/lox</sup>*Cd4*<sup>Cre</sup>) and *Trmt61a*-KO (*Trmt61a*<sup>lox/lox</sup>*RiboTag*<sup>lox/lox</sup>*Cd4*<sup>Cre</sup>) mice (activated with plate-bound anti-CD3 plus anti-CD28 in a 96-well plate for 6 h) and washed and treated with 100 μg ml<sup>-1</sup> cycloheximide for 1 min. Cells were washed in ice-cold PBS twice, and then RiboTag lysis buffer (containing cycloheximide, heparin and RNase inhibitor SupersaseIN) was added directly to the cells on ice as previously described<sup>38</sup>. Cell lysates were passed through a 26-gauge needle ten times and incubated for 30 min on ice to ensure complete

lysis. Ribosomal-RNA-containing supernatants were clarified by centrifugation at 12,000g for 10 min at 4°C. Haemagglutinin-conjugated magnetic beads (Pierce) were added to samples, followed by incubation overnight under gentle inversion at 4°C. Beads were washed three times for 10 min with gentle rotation in a high-salt buffer containing cycloheximide. RNA was eluted from HA-beads using Qiagen RLT buffer containing 2-mercaptoethanol and antifoaming DX reagent (Qiagen) by 30 s vortex pulsing. RNA was isolated using an RNeasy micro kit. RNA purity and quantification were evaluated using a NanoDrop 2000 spectrophotometer (Thermo Scientific, USA). RNA integrity was assessed using an Agilent 2100 Bioanalyzer (Agilent Technologies). RNA samples were transferred to OE Biotech Co., Ltd. for cDNA library preparation using an NEBNext Ultra II Directional RNA Library Prep Kit according to the manufacturer's instructions. Samples were sequenced using the Illumina NovaSeq 6000 platform.

**RiboTag RNA sequencing analysis.** Fastq files from RNA sequencing and RiboTag RNA sequencing were aligned to the mm10 genome using HISAT2 v.2.2.1, and then StringTie (v.2.2.1) was used to count the numbers of reads mapped to each gene. After normalization to FPKM values, we obtained the FPKM ratio of individual genes by dividing the ribosomal fractions over their inputs. Next, we performed a *t*-test to determine the differentially expressed genes between the WT and KO groups, using a cut-off of 0.05. Then, ggplot2 (<http://ggplot2.tidyverse.org/index.html>) was used to produce volcano plots.

**Polyribosome Real-time PCR.** We performed<sup>53</sup> ribosome profiling by strictly following the manual *Eukaryotic Polyribosome Profile Analysis*. Briefly, 100 million naive T cells were isolated from WT and *Trmt61a<sup>fllox/fllox</sup>Cd4<sup>Cre</sup>* mice (preliminary activation with plate-bound anti-CD3 and anti-CD28 in 96-well plates for 12 h), washed and treated with 100 µg ml<sup>-1</sup> cycloheximide for 1 min. After lysis, one-third of the cell lysate was used as input RNA; the remainder was subjected to 5–50% sucrose gradient centrifugation at 274,000g for 2 h at 4°C, and the polyribosome fractions were collected. The input RNAs and polyribosome RNAs were then isolated with an RNA Clean & Concentrator-25 kit (Zymo Research). Real-time PCR was used to detect gene TE.

**ChIP Real-time PCR.** Ten million naive CD4<sup>+</sup> T cells were isolated from WT mice and activated with plate-bound anti-CD3 plus anti-CD28 in a 96-well plate for 1 h. Cells were cross-linked, followed by the preparation of nuclear lysates using a ChIP-IT High Sensitivity kit (Active Motif). Nuclear lysates were sonicated to shear DNA to around 400 bp, followed by immunoprecipitation for 16 h at 4°C using IgG or anti-cJUN (Cell Signaling Technology, cat. no. 9165) and anti-FOSL2 (Abcam, cat. no. ab216838) antibodies. Genomic DNA corresponding to the *Trmt61a* promoter was quantified with SYBR Green reagents. The primers used for these analyses were as follows:

c-JUN forward 1: 5'-GGCAGACACTTCGTGCACC-3';  
 c-JUN reverse 1: 5'-CTGTGCAGGCTTGCACGTTG-3';  
 c-JUN forward 2: 5'-CAGGGACTTTTATTTCCGCACAG-3';  
 c-JUN reverse 2: 5'-CTGTCTTTGGCTGCTCCC-3';  
 FOSL2 forward: 5'-GGATATGCCACTCAGGTTGGTG-3';  
 FOSL2 reverse: 5'-GCAGTAGTCACAGTGGCATTCTG-3'.  
 c-JUN or FOSL2 binding was quantified after normalization to input DNA.

**Statistics.** No statistical methods were used to predetermine sample sizes, but our sample sizes were similar to those reported in previous publications. Samples or mice were grouped according to treatments or genotypes and thus were not randomized. Data collection and analysis were not performed blind to the conditions of the experiments. No data were excluded from the analyses. No tests for normality were performed; instead, the data distribution was assumed to be normal. Unless indicated otherwise, unpaired Student's *t*-test and two-way analysis of variance (ANOVA) were used to compare pairs of groups with GraphPad Prism 6. Data are expressed as the mean ± s.e.m. Values of *P* < 0.05 were considered to indicate statistical significance: \*\*\*\**P* < 0.0001, \*\*\**P* < 0.001, \*\**P* < 0.01, \**P* < 0.05. All in vivo experiments were conducted with at least two independent cohorts.

**Reporting summary.** Further information on research design is available in the Nature Research Reporting Summary linked to this article.

## Data availability

Source data are provided with this paper. All the high-throughput sequencing data generated for this study have been deposited in the NCBI Gene

Expression Omnibus (GEO) (<https://www.ncbi.nlm.nih.gov/geo/query/acc.cgi?acc=GSE184909>). The ChIP sequencing data are accessible from GEO with the following accession IDs: GSE39756, GSE40918, GSE54191, GSE58075 and GSE102317. The mass spectrometry proteomics data are available via the PRIDE database (<http://www.proteomexchange.org>) under accession numbers PXD004367 and PXD005492.

## Code availability

Detailed custom Python scripts are available at [https://github.com/xting1996/Proj\\_tRNA\\_m1A\\_in\\_T\\_cell](https://github.com/xting1996/Proj_tRNA_m1A_in_T_cell).

## References

- Jackson, R. et al. The translation of non-canonical open reading frames controls mucosal immunity. *Nature* **564**, 434–438 (2018).
- Yu, G., Wang, L. G., Han, Y. & He, Q. Y. clusterProfiler: an R package for comparing biological themes among gene clusters. *Omics* **16**, 284–287 (2012).
- Gu, Z., Eils, R. & Schlesner, M. Complex heatmaps reveal patterns and correlations in multidimensional genomic data. *Bioinformatics* **32**, 2847–2849 (2016).
- Esposito, A.M. et al. Eukaryotic polyribosome profile analysis. *J. Vis. Exp.* <https://doi.org/10.3791/1948> (2010).

## Acknowledgements

We thank M. Yang, K. Mao and Y. Zhou for technical and administrative assistance. We also thank all members of the H.-B.L. laboratory for discussion. This work was supported by the National Natural Science Foundation of China (82030042/32070917/82111540277 to H.-B.L., 31861143026/21825701/91940304 to C.Y., 81901580 to Y.L., 81901569 to J. Zhou and 32171283 to X.L.), the Chongqing International Institute for Immunology (2021YJC01 to H.-B.L.), the Ministry of Science and Technology of China (2021YFA1100800 to H.-B.L.), the National Key R&D Program of China (2019YFA0802200/2019YFA0110900 to C.Y.), Shanghai Science and Technology Commission (20JC1417400/201409005500 to H.-B.L., 20JC1410100 to J. Zheng and 20ZR1472900 to Y.Y.), the Shanghai Super Postdoctoral Program (Y.L. and J. Zhou), the China Postdoctoral Science Foundation (2019M651525 to Y.L. and 2020M671149 to J. Zhou), the Postdoctoral Innovation Talent Support Program (BX20190214 to J. Zhou), the Innovative Research Team of High-Level Local Universities in Shanghai (SHSMU-ZDCX20212501 to H.-B.L. and SHSMU-ZDCX20212500 to J. Zhou) and the Howard Hughes Medical Institute (R.A.F.).

## Author contributions

Y.L. designed the research, performed experiments and drafted the manuscript; J.Zhou performed experiments and revised the manuscript; X.L., X.Z. and J.S. performed experiments and the bioinformatic analysis; S.M., X.H., L.D., X.W. and H.L. performed experiments; H.C. and Y.Y. performed the bioinformatic analysis; G.R.L., J.Zheng., R.-J.L., B.S. and Y.Y. contributed to discussions and suggestions; R.A.F., C.Y. and Y.W. coordinated and revised the manuscript; and H.-B.L. conceived the project, designed the study, supervised the research, acquired the funding, and wrote and revised the manuscript.

## Competing interests

R.A.F. is a consultant for GSK and Zai Lab Ltd. All other authors declare no competing interests.

## Additional information

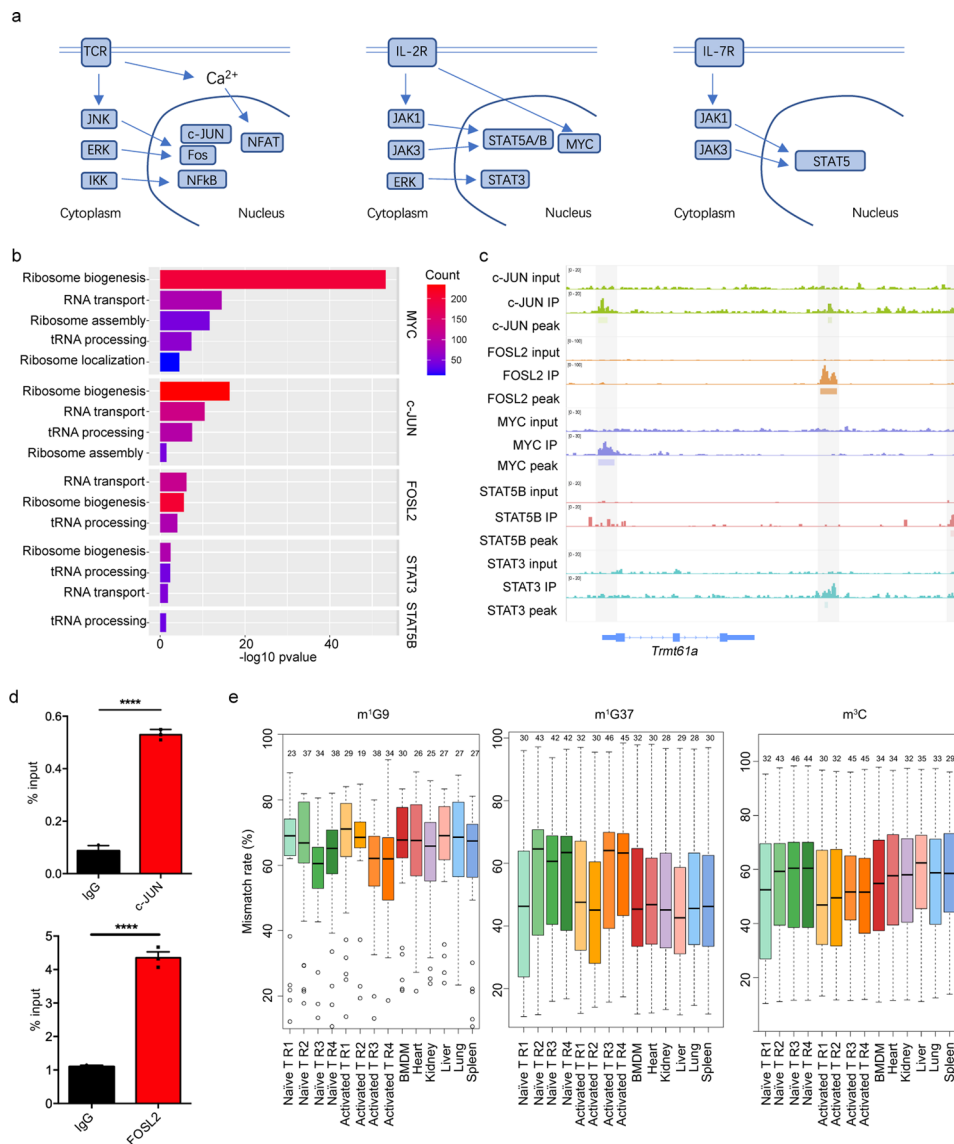
**Extended data** is available for this paper at <https://doi.org/10.1038/s41590-022-01301-3>.

**Supplementary information** The online version contains supplementary material available at <https://doi.org/10.1038/s41590-022-01301-3>.

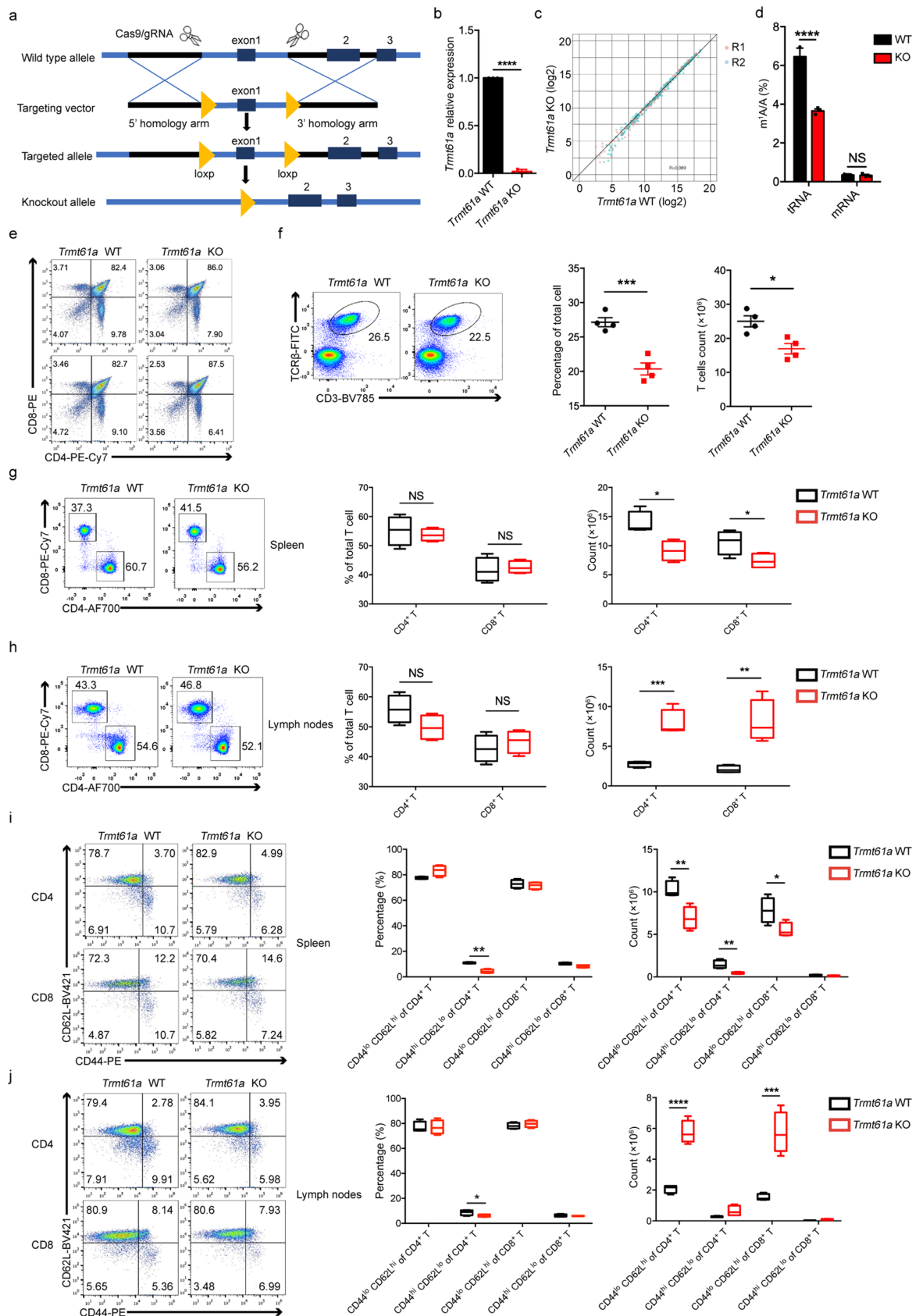
**Correspondence and requests for materials** should be addressed to Richard A. Flavell, Chengqi Yi, Yuzhang Wu or Hua-Bing Li.

**Peer review information** *Nature Immunology* thanks the anonymous reviewers for their contribution to the peer review of this work. Primary Handling Editor: L. A. Dempsey, in collaboration with the *Nature Immunology* team. Peer reviewer reports are available.

**Reprints and permissions information** is available at [www.nature.com/reprints](http://www.nature.com/reprints).

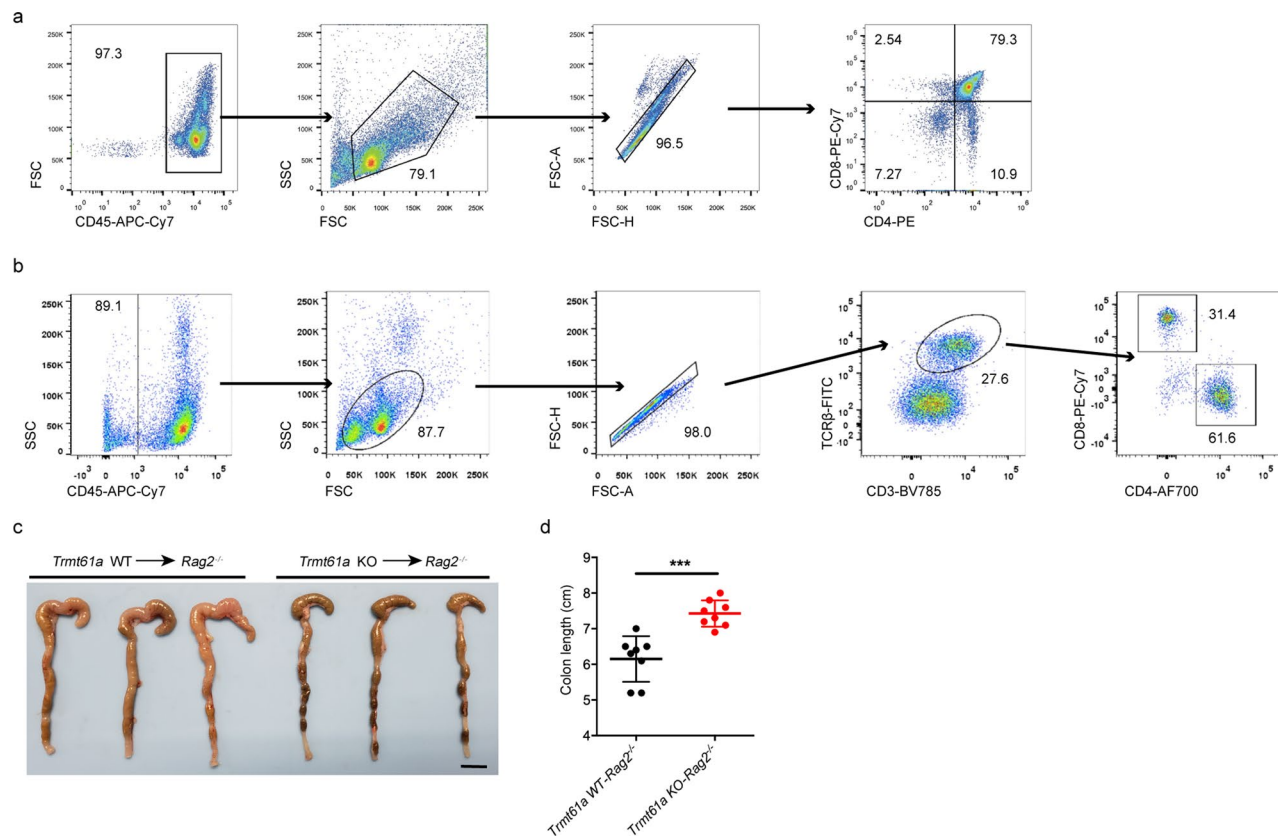


**Extended Data Fig. 1 | The transcriptional and translational regulation during T cell activation.** **a** The schematic diagram of the TCR, IL-2R, and IL-7R pathways during T cell activation. **b** GO analysis of the genes regulated by transcription factors MYC, c-JUN, FOSL2, STAT3, and STAT5B within T cell according to the published ChIP-seq data, pathways involved in translational regulation were listed, and the gene counts in different pathways were also indicated. Hypergeometric test (adjustments method: BH). **c** IGV snapshots showing the alignment data (BigWig format), including IP and input, around the *Trmt61a* gene loci for ChIP-seq experiments from public datasets. Labels indicate some genomic regions with peaks. **d** Validation of the interaction between c-JUN or FOSL2 and the *Trmt61a* gene. c-JUN or FOSL2 binding was quantified after normalization to input DNA (%input =  $100 \times 2^{-\text{Ct}_{\text{adjusted}} - \text{Ct}_{\text{target}}}$ ). Error bars represent mean  $\pm$  s.e.m.,  $n = 3$  biologically independent samples. \*\*\*\* $P < 0.0001$ , two-tailed, unpaired  $t$ -test. **e** Quantification of the m<sup>1</sup>G9/G9, m<sup>1</sup>G37/G37, m<sup>3</sup>C/C ratios in total tRNA purified from naïve CD4<sup>+</sup> T cells, in vitro activated CD4<sup>+</sup> T cells (24 hours), BMDMs, heart, kidney, liver, lung, and spleen by tRNA-sequencing. Data are shown as box plots (The  $n$  number is displayed above boxes and boxes show median, upper and lower quartiles, whiskers show 1.5 $\times$  IQR on either side, and the points show outlier).

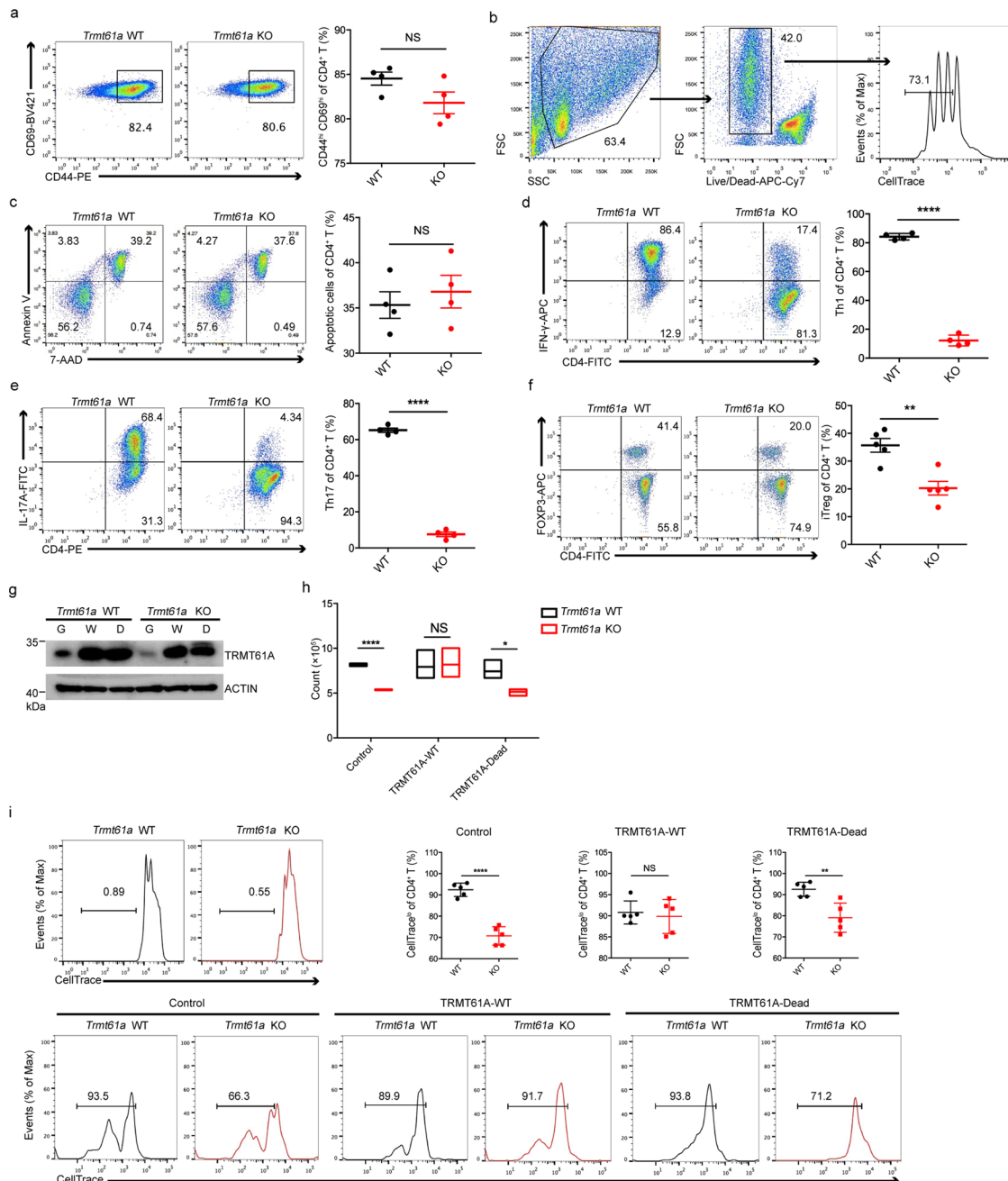


Extended Data Fig. 2 | See next page for caption.

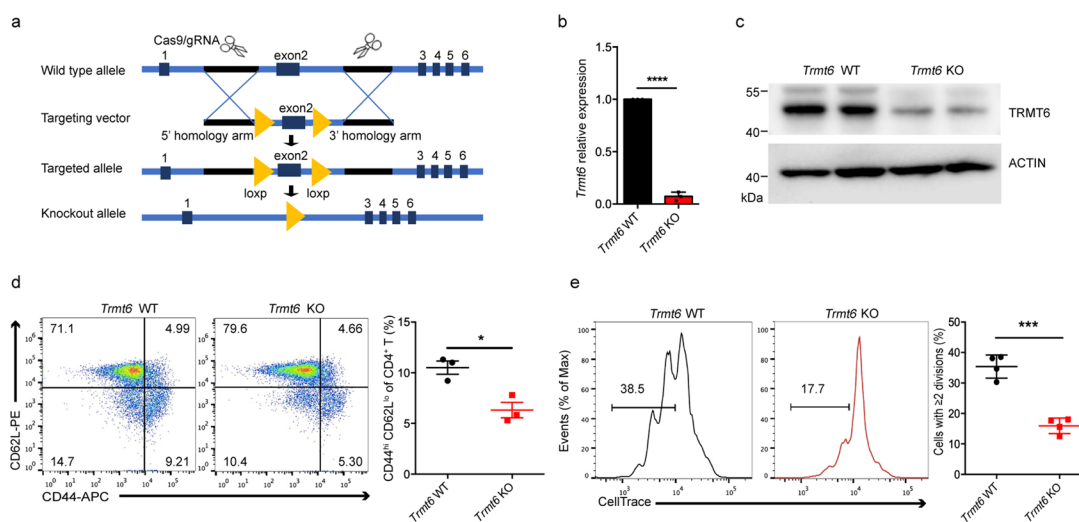
**Extended Data Fig. 2 | Characterization of *Trmt61a* conditional knockout mice.** **a.** The schematic diagram of the generation of *Trmt61a* conditional knockout mice. **b.** The mRNA level of *Trmt61a* was analyzed by real-time PCR in *Trmt61a*-KO and WT naïve CD4<sup>+</sup> T cells. Error bars represent mean  $\pm$  s.e.m.,  $n=3$  biologically independent samples from 3 independent experiments. \*\*\*\*  $P < 0.0001$ ; two-tailed, unpaired  $t$ -test. **c.** tRNA-seq detection of the level of each tRNA in activated *Trmt61a*-KO CD4<sup>+</sup> T cells and WT CD4<sup>+</sup> T cells (6 hours). Each dot represents one tRNA. Two biologically independent samples are shown (R1, R2). **d.** Quantification of the m<sup>1</sup>A/A ratio in tRNA and mRNA by liquid chromatography-mass spectrometry. Error bars represent mean  $\pm$  s.e.m.,  $n=3$  biologically independent samples. \*\*\*\*  $P < 0.0001$ ; NS: non-significant; two-tailed, unpaired  $t$ -test. **e.** The development of T cells in the thymus of 8-week-old *Trmt61a*-KO mice and littermate control mice. Representative data of six independent experiments are shown. **f.** The percentage and cell number of T cells (CD3<sup>+</sup> TCR $\beta$ <sup>+</sup>) were quantified. Error bars represent mean  $\pm$  s.e.m.,  $n=4$  biologically independent animals. \*\*\*  $P = 0.0008$ , \*  $P = 0.0111$ ; two-tailed, unpaired  $t$ -test. **g.** The percentage and cell number of CD4<sup>+</sup> or CD8<sup>+</sup> T cells in spleen were quantified. \*  $P = 0.0100$  (CD4), \*  $P = 0.0385$  (CD8), NS: non-significant; two-tailed, unpaired  $t$ -test. **h.** The percentage and cell number of CD4<sup>+</sup> or CD8<sup>+</sup> T cells in lymph nodes were quantified. \*\*\*  $P = 0.0008$ , \*\*  $P = 0.0046$ , NS: non-significant; two-tailed, unpaired  $t$ -test. **i.** The fractions of effector memory cells (CD44<sup>hi</sup>CD62L<sup>lo</sup>) and naïve cells (CD44<sup>lo</sup>CD62L<sup>hi</sup>) in spleen were quantified. \*\*  $P = 0.0069$ , \*  $P = 0.0356$ ; two-tailed, unpaired  $t$ -test. **j.** The fractions of effector memory cells (CD44<sup>hi</sup>CD62L<sup>lo</sup>) and naïve cells (CD44<sup>lo</sup>CD62L<sup>hi</sup>) in lymph nodes were quantified. \*\*\*\*  $P < 0.0001$ , \*\*\*  $P = 0.0008$ , \*  $P = 0.0732$ ; two-tailed, unpaired  $t$ -test. Boxes show median, upper and lower quartiles, whiskers show 1.5 $\times$  IQR on either side (**g-j**).  $n=4$  biologically independent animals (**g-j**).



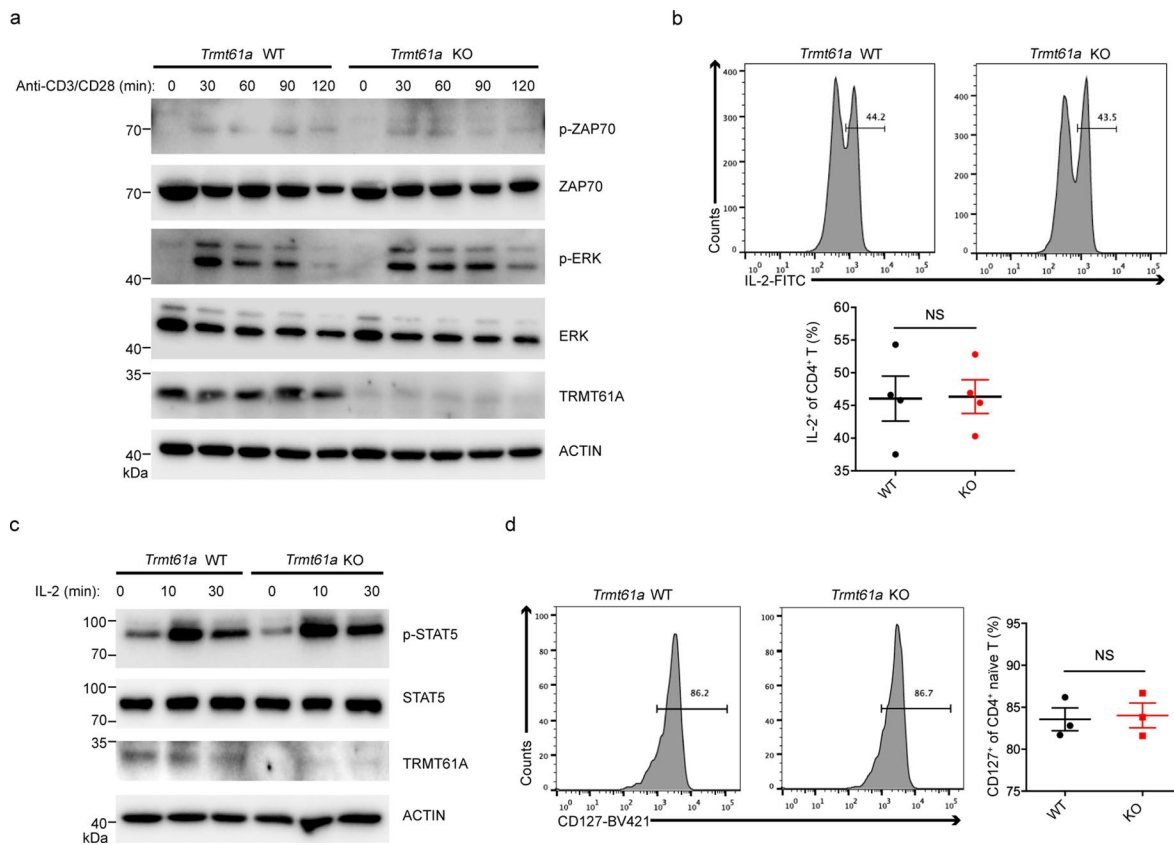
**Extended Data Fig. 3 | *Trmt61a* KO T cells failed to induce adoptive transfer colitis.** **a.** Representative flow cytometry gating strategy for thymocyte. **b.** Representative flow cytometry gating strategy for CD4<sup>+</sup> T cell and CD8<sup>+</sup> T cell in spleen or lymph nodes. **c.** Representative image of the colons from *Rag2*<sup>-/-</sup> mice receiving WT or *Trmt61a*-KO naïve CD4<sup>+</sup> T cells 12 weeks post-transfer. Scale bars, 1cm. **d.** The length of colons from *Rag2*<sup>-/-</sup> mice receiving WT or *Trmt61a*-KO naïve CD4<sup>+</sup> T cells 12 weeks post-transfer. Error bars represent mean  $\pm$  s.e.m.,  $n = 8$  biologically independent animals. \*\*\*  $P = 0.0002$ ; two-tailed, unpaired  $t$ -test.



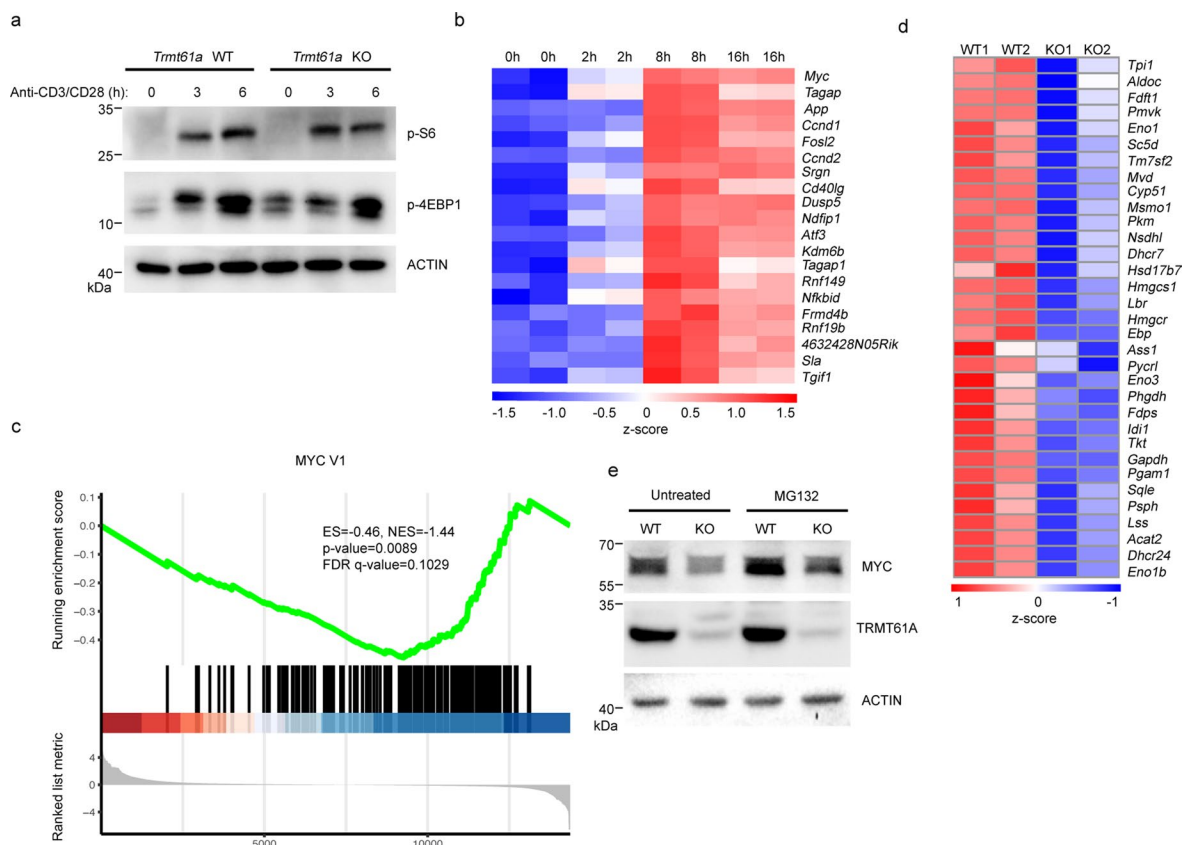
**Extended Data Fig. 4 | Characterization of *Trmt61a* KO T cells *in vitro*.** **a.** The T cell activation was assessed by flow cytometry analysis of CD69 and CD44 staining. Quantification of the fraction of activated T cells (CD69<sup>hi</sup>CD44<sup>hi</sup>) was shown in the right graph. Error bars represent mean  $\pm$  s.e.m.,  $n = 4$  biologically independent samples. NS: non-significant; two-tailed, unpaired *t*-test. **b.** Representative flow cytometry gating strategy for CellTrace dilution in CD4<sup>+</sup> T cell. **c.** Apoptosis was assessed by flow cytometry after staining by Annexin V and 7-AAD. The percentage is listed in the right graph. Error bars represent mean  $\pm$  s.e.m.,  $n = 4$  biologically independent samples. NS: non-significant; two-tailed, unpaired *t*-test. **d.** Naïve CD4<sup>+</sup> T cells were differentiated into Th1 subset under defined optimal conditions. The percentage is listed in the right graph. Error bars represent mean  $\pm$  s.e.m.,  $n = 4$  biologically independent samples. \*\*\*\*  $P < 0.0001$ ; two-tailed, unpaired *t*-test. **e.** Naïve CD4<sup>+</sup> T cells were differentiated into Th17 subset under defined optimal conditions. The percentage is listed in the right graph. Error bars represent mean  $\pm$  s.e.m.,  $n = 4$  biologically independent samples. \*\*\*\*  $P < 0.0001$ ; two-tailed, unpaired *t*-test. **f.** Naïve CD4<sup>+</sup> T cells were differentiated into iTreg subset under defined optimal conditions. The percentage is listed in the right graph. Error bars represent mean  $\pm$  s.e.m.,  $n = 5$  biologically independent samples. \*\*  $P = 0.0022$ ; two-tailed, unpaired *t*-test. **g.** Retrovirus-mediated expression of TRMT61A-WT and TRMT61A-Dead in WT and *Trmt61a*-KO CD4<sup>+</sup> T cells. The protein level of TRMT61A was quantified by immunoblot. G: EGFP, W: TRMT61A-WT, D: TRMT61A-Dead. Representative data of three independent experiments are shown. **h.** Flow cytometric analysis of cell counts. Data are shown as box plots (boxes show median, upper and lower quartiles, whiskers show 1.5 $\times$  IQR on either side).  $n = 3$  biologically independent samples. \*\*\*\*  $P < 0.0001$ , \*  $P = 0.0267$ , NS: non-significant; two-tailed, unpaired *t*-test. **i.** Up left: CellTrace dilution in WT and *Trmt61a* KO CD4<sup>+</sup> T cells before transfer; Up right: flow cytometric analysis of CellTrace dilution in different treatments; Down: flow cytometry shows CellTrace dilution in different treatments. Error bars represent mean  $\pm$  s.e.m.,  $n = 5$  biologically independent samples. \*\*\*\*  $P < 0.0001$ , \*\*  $P = 0.0045$ , NS: non-significant; two-tailed, unpaired *t*-test.



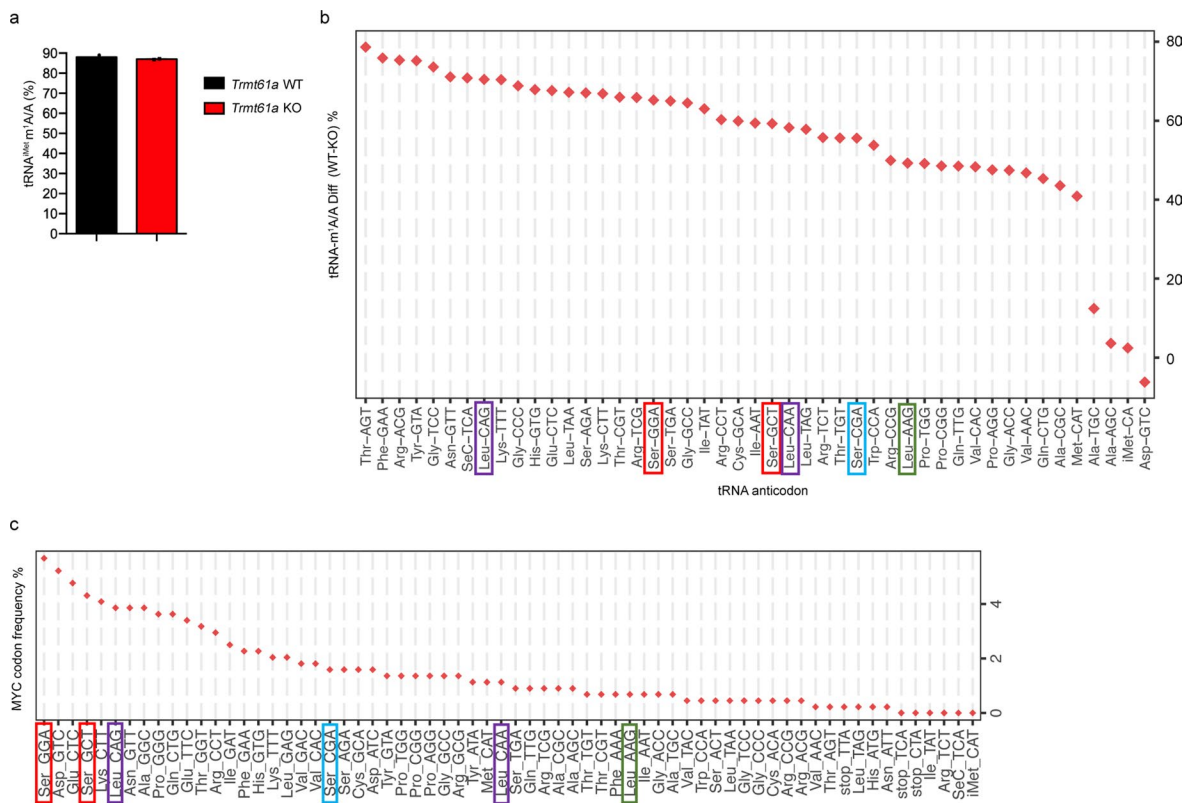
**Extended Data Fig. 5 | Characterization of *Trmt6* conditional knockout mice.** **a** The schematic diagram of the generation of *Trmt6* conditional knockout mice. **b** The mRNA level of *Trmt6* was analyzed by real-time PCR in *Trmt6*-KO and WT naive CD4<sup>+</sup> T cells. Error bars represent mean  $\pm$  s.e.m.,  $n = 3$  biologically independent samples from 3 independent experiments. \*\*\*\*  $P < 0.0001$ ; two-tailed, unpaired  $t$ -test. **c** The protein level of TRMT6 was quantified by immunoblot in *Trmt6*-KO and WT naive CD4<sup>+</sup> T cells. Representative data of three independent experiments are shown. **d** CD4<sup>+</sup> T cell subpopulations from the spleens of 8-week-old *Trmt6*-KO mice and littermate control mice were analyzed by flow cytometry. The fraction of CD4<sup>+</sup> effector memory cells (CD44<sup>hi</sup>CD62L<sup>lo</sup>) was quantified. Error bars represent mean  $\pm$  s.e.m.,  $n = 3$  biologically independent animals. \*  $P = 0.0140$ ; two-tailed, unpaired  $t$ -test. **e** The proliferation of WT naive CD4<sup>+</sup> T cells and *Trmt6*-KO naive CD4<sup>+</sup> T cells in the presence of anti-CD3 and anti-CD28 antibodies, as measured by CellTrace dilution after 3 days. Error bars represent mean  $\pm$  s.e.m.,  $n = 4$  biologically independent samples. \*\*\*  $P = 0.0001$ ; two-tailed, unpaired  $t$ -test.



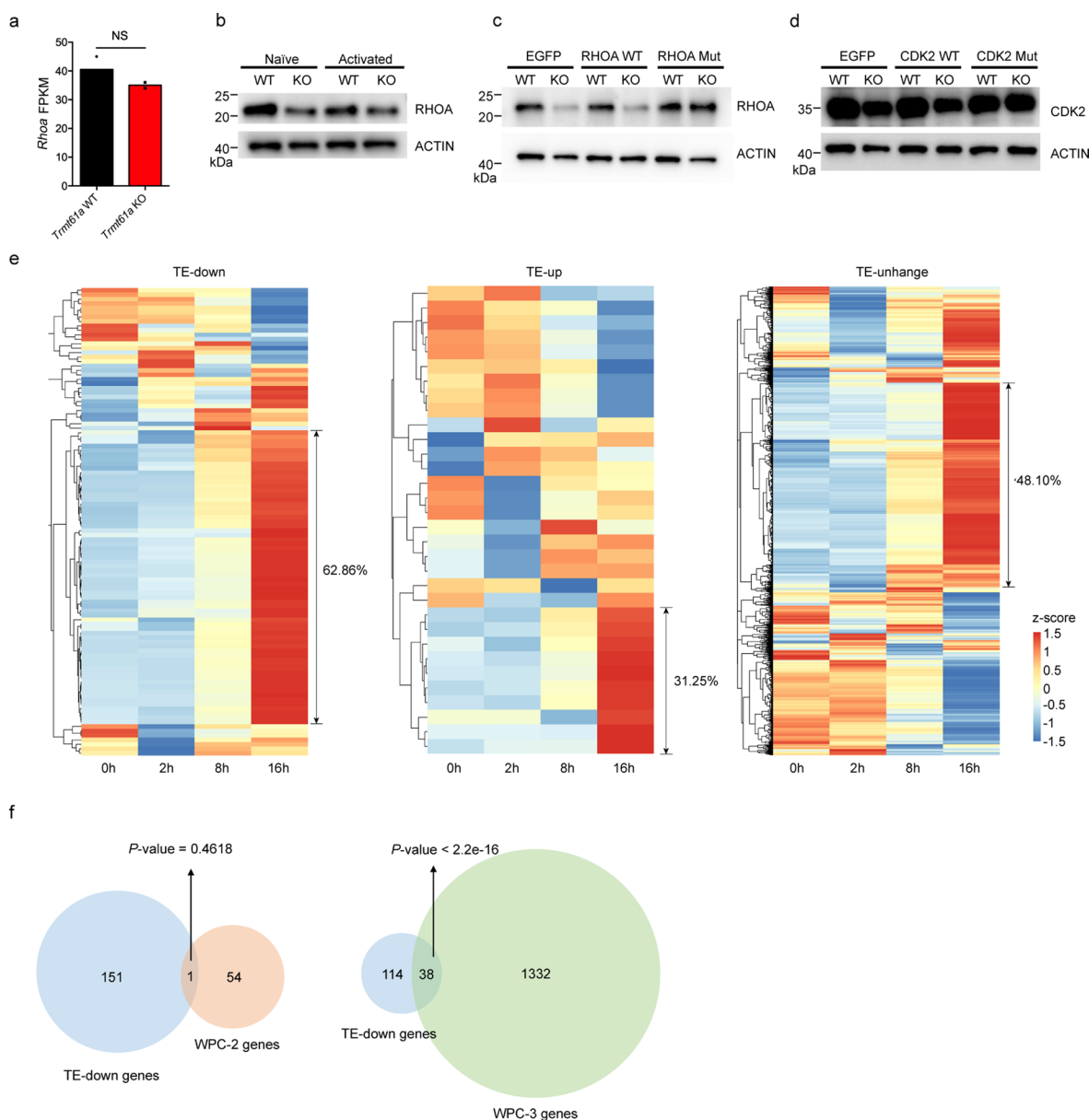
**Extended Data Fig. 6 | Deletion *Trmt61a* did not affect the TCR/IL-2 signaling pathway. a.** Naïve CD4<sup>+</sup> T cells obtained from the spleens of *Trmt61a*-KO and littermate control mice were stimulated for the indicated minutes with anti-CD3 and anti-CD28 antibodies. Phosphorylated proteins of the TCR signaling pathway were detected by immunoblot. Representative data of two independent experiments are shown. **b.** Naïve CD4<sup>+</sup> T cells obtained from the spleens of *Trmt61a*-KO and littermate control mice were stimulated for 24 hours with anti-CD3 and anti-CD28 antibodies. The expression of IL-2 was quantified by flow cytometry. Error bars represent mean  $\pm$  s.e.m.,  $n = 4$  biologically independent samples. NS: non-significant; two-tailed, unpaired  $t$ -test. **c.** CD4<sup>+</sup> T cells obtained from the spleens of *Trmt61a*-KO and littermate control mice were stimulated for the indicated times with IL-2. The phosphorylation of STAT5 in the IL-2 signaling pathway was detected by immunoblot. Representative data of two independent experiments are shown. **d.** Naïve CD4<sup>+</sup> T cells were obtained from the spleens of *Trmt61a*-KO and littermate control mice. The expression of CD127 was quantified by flow cytometry. Error bars represent mean  $\pm$  s.e.m.,  $n = 3$  biologically independent samples. NS: non-significant; two-tailed, unpaired  $t$ -test.



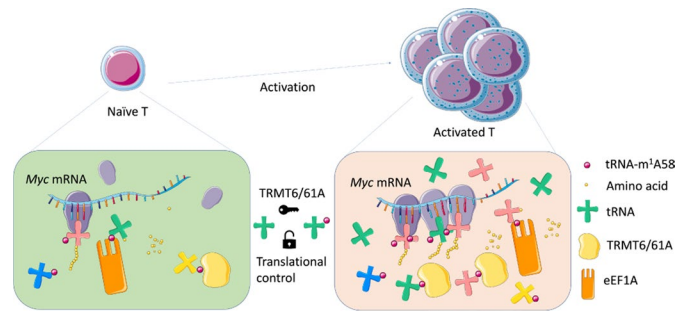
**Extended Data Fig. 7 | mTOR signaling and MYC pathways.** **a.** Naïve CD4<sup>+</sup> T cells obtained from the spleens of *Trmt61a*-KO and littermate control mice were stimulated for the indicated times with anti-CD3 and anti-CD28 antibodies. Phosphorylated proteins of the mTORC1 signaling pathway were detected by immunoblot. Representative data of four independent experiments are shown. **b.** Heatmap showing the expression of proteins in activated CD4<sup>+</sup> T cells for indicated timepoint, data from the PRIDE database under accession numbers PXD004367. **c.** Gene-set enrichment analysis showing the down-regulated genes in *Trmt61a*-KO cells involved in MYC signaling. **d.** Heatmap showing the expressions of transcripts of the cholesterol biosynthesis and amino acid biosynthesis pathways in activated *Trmt61a*-KO CD4<sup>+</sup> T cells vs. activated WT CD4<sup>+</sup> T cells (anti-CD3 and anti-CD28 antibodies for 48 hours). **e.** Naïve CD4<sup>+</sup> T cells obtained from the spleens of *Trmt61a*-KO and littermate control mice were stimulated for 3 hours with anti-CD3 and anti-CD28 antibodies and then treated by MG132 for 3 hours. The level of MYC protein was quantified by immunoblot. Representative data of two independent experiments are shown.



**Extended Data Fig. 8 | The design principle of codon switch assay. a.** tRNA-m<sup>A</sup>-seq detection of the m<sup>A</sup>A58 modification level of tRNA<sup>Met</sup> in activated *Trmt61a*-KO CD4<sup>+</sup> T cells and WT CD4<sup>+</sup> T cells (6 hours). n = 2 biologically independent samples. **b.** The decrease in magnitude (the tRNA-m<sup>A</sup>58 level in WT CD4<sup>+</sup> T cells minus the level in KO CD4<sup>+</sup> T cells) of the tRNA-m<sup>A</sup>58 level in each tRNA after TRMT61A deletion. **c.** The codon frequency of mouse *Myc* mRNA. In the *Myc* codon switch assay, the codons marked with red boxes were replaced with the codon marked with blue box, and the codons marked with purple boxes were replaced with the codon marked with green box.



**Extended Data Fig. 9 | The protein levels of TE down-regulated mRNAs.** **a.** Naïve CD4<sup>+</sup> T cells were activated with 5 µg/mL anti-CD3 antibody and 2 µg/mL anti-CD28 antibody for 6 hours. The expression of *Rhoa* was verified by RNA sequencing.  $n=2$  biologically independent samples. NS: non-significant; two-tailed, unpaired *t*-test. **b.** Naïve CD4<sup>+</sup> T cells obtained from the spleens of *Trmt61a*-KO and littermate control mice were stimulated for the indicated times with anti-CD3 and anti-CD28 antibodies (6 hours). The representative target with TE-downregulation was verified by immunoblot. Representative data of three independent experiments are shown. **c.** Retrovirus-mediated expression of RHOA-WT and RHOA-Mutant (All Leu codons replaced by CTT, and all Gly codons replaced by GGT) in WT and *Trmt61a*-KO CD4<sup>+</sup> T cells. The protein level of RHOA was quantified by immunoblot. Representative data of two independent experiments are shown. **d.** Retrovirus-mediated expression of CDK2-WT and CDK2-Mutant (All Leu codons replaced by CTT, all His codons replaced by CAT, and all Gly codons replaced by GGT) in WT and *Trmt61a*-KO CD4<sup>+</sup> T cells. The protein level of CDK2 was quantified by immunoblot. Representative data of two independent experiments are shown. **e.** Heatmap showing the protein expression of TE-down, TE-up, and TE-unchange transcripts in *Trmt61a*-KO activated CD4<sup>+</sup> T cells (6 hours), data obtained from the PRIDE database under accession numbers [PXD004367](https://proteomecentral.proteomexchange.org/id/PXD004367). **f.** Venn diagram showed the intersection of the TE-down genes in RiboTag RNA-seq and genes in WPC-2 or WPC-3 (WPC-2 and WPC-3 were obtained from PMID: 28285833). The *P* value of intersection was calculated by the fisher test (two-sided).



**Extended Data Fig. 10 | The m<sup>1</sup>A58 in tRNA promotes *Myc* mRNA translation in activated CD4<sup>+</sup> T cells.** Proposed mechanistic model depicting tRNA-m<sup>1</sup>A58 mediated translational control during T cell activation.

## Reporting Summary

Nature Portfolio wishes to improve the reproducibility of the work that we publish. This form provides structure for consistency and transparency in reporting. For further information on Nature Portfolio policies, see our [Editorial Policies](#) and the [Editorial Policy Checklist](#).

### Statistics

For all statistical analyses, confirm that the following items are present in the figure legend, table legend, main text, or Methods section.

n/a Confirmed

- The exact sample size ( $n$ ) for each experimental group/condition, given as a discrete number and unit of measurement
- A statement on whether measurements were taken from distinct samples or whether the same sample was measured repeatedly
- The statistical test(s) used AND whether they are one- or two-sided  
*Only common tests should be described solely by name; describe more complex techniques in the Methods section.*
- A description of all covariates tested
- A description of any assumptions or corrections, such as tests of normality and adjustment for multiple comparisons
- A full description of the statistical parameters including central tendency (e.g. means) or other basic estimates (e.g. regression coefficient) AND variation (e.g. standard deviation) or associated estimates of uncertainty (e.g. confidence intervals)
- For null hypothesis testing, the test statistic (e.g.  $F$ ,  $t$ ,  $r$ ) with confidence intervals, effect sizes, degrees of freedom and  $P$  value noted  
*Give  $P$  values as exact values whenever suitable.*
- For Bayesian analysis, information on the choice of priors and Markov chain Monte Carlo settings
- For hierarchical and complex designs, identification of the appropriate level for tests and full reporting of outcomes
- Estimates of effect sizes (e.g. Cohen's  $d$ , Pearson's  $r$ ), indicating how they were calculated

*Our web collection on [statistics for biologists](#) contains articles on many of the points above.*

### Software and code

Policy information about [availability of computer code](#)

Data collection

1. RNA/ tRNA sequencing data were sequenced by the Illumina HiSeq X10 platform.
2. RiboTag RNA sequencing data were sequenced using the Illumina Novaseq6000 platform.
2. Liquid chromatography-mass spectrometry (LC-MS) /MS data were collected with triple-quadrupole mass spectrometer (AB SCIEX QTRAP 5500).
3. RT-qPCR data were collected with Bio-Rad CFX Connect Real-Time System (Bio-Rad CFX Maestro 1.1).
4. Immunoblots were collected with Bio-Rad ChemiDoc™ Imaging System (12003153).
5. Flow cytometry data were collected with BD LSRFortessa X20.

## Data analysis

1. For flow cytometry, FlowJo (vX.0.7) was used. Numerical data were exported to Excel (16.54) and were further analyzed by using GraphPad Prism (Version 6.0c).
2. For RNA-seq, Index of the reference genome was built using Hisat2 (v2.0.5) and paired-end clean reads were aligned to the mm10 genome using Hisat2 (v2.0.5), and then featureCounts (v1.5.0-p3) was used to count the reads numbers mapped to each gene. For Ribo-seq, the rRNA removed reads of each sample were mapped to the reference genome by Bowtie2(V 2.4.1) allowing no mismatches. For m1A-seq, clean reads were mapped to mm10 tRNA genome by bowtie2. For RiboTag-seq, the Index of the reference genome was built using Hisat2 (v2.2.1) and paired-end clean reads were aligned to the mm10 genome using Hisat2 (v2.2.1), and then Stringtie (v2.2.1) was used to count the reads numbers mapped to each gene.
3. For tRNA m1A-seq analysis. Raw reads adapter sequences were trimmed by trim galore (version 0.6.5), the minimum quality threshold was set to 20, and the minimum length required for reads after trimming was 30 nt. The remaining reads were further processed by removing the first 10 nt random barcode in the 5' end. Processed reads were mapped to mouse Transfer RNA (tRNA) reference (<http://gtrnadb.ucsc.edu/genomes/eukaryota/Mmus10/Mmus10-seq.html>) using BWA-MEM with default parameters.
4. Graphpad prism 6 (Version 6.0c) and Excel (16.54) was used to analyze the RT-qPCR data.
5. Sequencing data was analyzed using the Snppgene (4.1.6).

For manuscripts utilizing custom algorithms or software that are central to the research but not yet described in published literature, software must be made available to editors and reviewers. We strongly encourage code deposition in a community repository (e.g. GitHub). See the Nature Portfolio [guidelines for submitting code & software](#) for further information.

## Data

Policy information about [availability of data](#)

All manuscripts must include a [data availability statement](#). This statement should provide the following information, where applicable:

- Accession codes, unique identifiers, or web links for publicly available datasets
- A description of any restrictions on data availability
- For clinical datasets or third party data, please ensure that the statement adheres to our [policy](#)

All the high-throughput sequencing data generated for this study has been deposited in the NCBI Gene Expression Omnibus (GEO) (<https://www.ncbi.nlm.nih.gov/geo/query/acc.cgi?acc=GSE184909>).

The Chip-seq data are accessible from Gene Expression omnibus (GEO) with the following accession ID: GSE39756, GSE40918, GSE54191, GSE58075, GSE102317.

The mass spectrometry proteomics data are available via the PRIDE database (<http://www.proteomexchange.org>) under accession numbers PXD004367 and PXD005492.

## Field-specific reporting

Please select the one below that is the best fit for your research. If you are not sure, read the appropriate sections before making your selection.

Life sciences  Behavioural & social sciences  Ecological, evolutionary & environmental sciences

For a reference copy of the document with all sections, see [nature.com/documents/nr-reporting-summary-flat.pdf](https://www.nature.com/documents/nr-reporting-summary-flat.pdf)

## Life sciences study design

All studies must disclose on these points even when the disclosure is negative.

Sample size	No statistical methods were used to pre-determine sample sizes but our sample sizes are similar to those reported in previous publications.
Data exclusions	No data were excluded from the analyses.
Replication	Replication are indicated in the figure legends. Independent experiment and biological replicate were used to ensure the reproducibility of results.
Randomization	Samples or mice were grouped according to treatment or genotypes, and thus not randomized.
Blinding	Data collection and analysis were not performed blind to the conditions of the experiments.

## Reporting for specific materials, systems and methods

We require information from authors about some types of materials, experimental systems and methods used in many studies. Here, indicate whether each material, system or method listed is relevant to your study. If you are not sure if a list item applies to your research, read the appropriate section before selecting a response.

## Materials &amp; experimental systems

## Methods

n/a	Involved in the study
<input type="checkbox"/>	<input checked="" type="checkbox"/> Antibodies
<input type="checkbox"/>	<input checked="" type="checkbox"/> Eukaryotic cell lines
<input checked="" type="checkbox"/>	<input type="checkbox"/> Palaeontology and archaeology
<input type="checkbox"/>	<input checked="" type="checkbox"/> Animals and other organisms
<input checked="" type="checkbox"/>	<input type="checkbox"/> Human research participants
<input checked="" type="checkbox"/>	<input type="checkbox"/> Clinical data
<input checked="" type="checkbox"/>	<input type="checkbox"/> Dual use research of concern

n/a	Involved in the study
<input checked="" type="checkbox"/>	<input type="checkbox"/> ChIP-seq
<input type="checkbox"/>	<input checked="" type="checkbox"/> Flow cytometry
<input checked="" type="checkbox"/>	<input type="checkbox"/> MRI-based neuroimaging

## Antibodies

## Antibodies used

Anti-mouse CD3 $\epsilon$  (145-2C11) FITC Biolegend Cat# 100306; Lot: B241616; RRID:AB\_312671; 1:200  
 Anti-mouse CD25 (3C7) PE Biolegend Cat# 101904; Lot: B238380; RRID:AB\_312847; 1:200  
 Anti-mouse CD62L (MEL-14) PE Biolegend Cat# 104408; Lot: B242686; RRID:AB\_313095; 1:200  
 Anti-mouse CD8 (53-6.7) PE Biolegend Cat# 100708; Lot: B243039; RRID:AB\_312747; 1:200  
 Anti-mouse CD8 (53-6.7) PE-Cy7 Biolegend Cat# 100722; Lot: B239088; RRID:AB\_312761; 1:200  
 Anti-mouse CD4 (GK1.5) PE-Cy7 Biolegend Cat# 100422; Lot: B224943; RRID:AB\_312707; 1:200  
 Anti-mouse CD3 (145-2C11) BV785 Biolegend Cat# 100355; Lot: B346637; RRID:AB\_2565969; 1:200  
 Anti-mouse TCR- $\beta$  (H57-597) FITC Biolegend Cat# 109206; RRID:AB\_313429; 1:200  
 Anti-mouse TCR- $\beta$  (H57-597) BV421 Biolegend Cat# 109234; Lot: B302703; RRID:AB\_2562350; 1:200  
 Anti-mouse CD4 (GK1.5) Alexa Fluor 700 Biolegend Cat# 100430; Lot: B331561; RRID:AB\_493699; 1:200  
 Anti-mouse CD4 (RM4-5) FITC Biolegend Cat# 100510; Lot: B324527; RRID:AB\_312713; 1:200  
 Anti-mouse CD4 (RM4-4) PE Biolegend Cat# 116006; Lot: B211830; RRID:AB\_313691; 1:200  
 Anti-mouse CD25 (3C7) FITC Biolegend Cat# 101908; RRID:AB\_961212; 1:200  
 Anti-mouse CD69 (H1.2F3) BV421 Biolegend Cat#104528; RRID:AB\_2562328; 1:200  
 Anti-mouse IFN- $\gamma$  (XMG1.2) APC Biolegend Cat# 505810 ; Lot: B299238; RRID:AB\_315404; 1:200  
 Anti-mouse IL-17A (TC11-18H10.1) FITC Biolegend Cat# 506908 ; Lot: B259285; RRID:AB\_536010; 1:200  
 Anti-mouse CD44 (IM7) APC Biolegend Cat# 103012 ; Lot: B240355; RRID:AB\_312963; 1:200  
 Anti-mouse IL-2 (JES6-5H4) FITC Biolegend Cat# 503806 ; Lot: B272441; RRID:AB\_315300; 1:200  
 Anti-mouse CD127 (A7R34) BV421 Biolegend Cat# 135024 ; Lot: B277509; RRID:AB\_11218800; 1:200  
 Anti-mouse CD45RB (C363-16A) APC Biolegend Cat# 103320 ; Lot: B210345 RRID:AB\_2565229; 1:200  
 Anti-mouse CD45 (30-F11) APC-CY7 Biolegend Cat# 103116; RRID:AB\_312981; 1:200  
 Anti-mouse CD44 (IM7) PE-Cy7 Biolegend Cat# 103030; Lot: B220566; RRID:AB\_830787; 1:200  
 Anti-mouse CD62L (MEL-14) BV421 Biolegend Cat# 104436; RRID:AB\_2562560; 1:200  
 Anti-mouse CD45RB (C363-16A) PerCP-Cy5.5 Biolegend Cat# 103314; RRID:AB\_2284707; 1:200  
 Anti-mouse TCR- $\beta$  (H57-597) PE-CY7 Biolegend Cat# 109222; Lot: B336462; RRID:AB\_893625; 1:200  
 Anti-mouse TCR- $\beta$  (H57-597) APC-CY7 Biolegend Cat# 109220; RRID:AB\_893624; 1:200  
 Anti-mouse CD3 $\epsilon$  (145-2C11) PE-CY7 Biolegend Cat# 100320; Lot: B316240; RRID:AB\_312685; 1:200  
 Anti-mouse CD3 $\epsilon$  (145-2C11) APC-CY7 Biolegend Cat# 100330; RRID:AB\_1877170;  
 Anti-mouse CD4 (GK1.5) BV711 Biolegend Cat# 100447; RRID:AB\_2564586; 1:200

Anti-mouse CD69 (H1.2F3) APC Biolegend Cat# 104514; Lot: B244020;  
 RRID:AB\_492843; 1:200  
 Anti-mouse Foxp3 (FJK-16s) APC Thermo Fisher Scientific Cat# 17-5773-80; Lot: 2152040;  
 RRID:AB\_469456; 1:200  
 Anti-mouse IFN- $\gamma$  (XMG1.2) Alexa Fluor 700 Biolegend Cat# 505824;  
 RRID:AB\_2561300; 1:200  
 Anti-mouse IL-17A (TC11-18H10.1) Alexa Fluor 647 Biolegend Cat# 506912;  
 RRID:AB\_536014; 1:200  
 Anti-mouse Ki-67 (16A8) BV421 Biolegend Cat# 652411;  
 RRID:AB\_2562663; 1:200  
 Anti-mouse CD8a (53-6.7) BV605 Biolegend Cat# 100744;  
 RRID:AB\_2562609; 1:200  
 Anti-mouse CD44 (IM7) PE Biolegend Cat# 103008; Lot: B334370;  
 RRID:AB\_312959; 1:200  
 Anti-mouse CD8a (53-6.7) PerCP-Cy5.5 Biolegend Cat# 100734; Lot: B313041;  
 RRID:AB\_2075238; 1:200  
 Anti-mouse IFN- $\gamma$  (XMG1.2) PE Biolegend Cat# 505808; Lot: B295804;  
 RRID:AB\_315402; 1:200  
 Anti-mouse TRMT61A antibody Thermo Fisher Scientific Cat# PA5-76553; Lot:31134A07;  
 RRID:AB\_2720280; 1:2000  
 Anti-mouse TRMT6 antibody Proteintech Cat# 16727-1-AP;  
 RRID:AB\_2878306; Lot: 00008101; 1:2000  
 Anti-mouse MYC antibody Proteintech Cat# 10828-1-AP;  
 RRID:AB\_2148585; 1:2000  
 Anti-mouse c-JUN antibody Cell Signaling Technology Cat# 9165; Lot: 13;  
 RRID:AB\_2130165; 1:2000  
 Anti-mouse FOSL2 antibody abcam Cat# ab216838; 1:2000  
 Anti-mouse RHOA antibody Cell Signaling Technology Cat# 2117;  
 RRID:AB\_10693922; Lot: 5; 1:2000  
 Anti-mouse Cyclin-E1 antibody Proteintech Cat# 11554-1-AP; Lot: 00047453;  
 RRID:AB\_2071066; 1:2000  
 Anti-mouse Cdk2 antibody abcam Cat# ab32147;  
 RRID:AB\_726775; 1:2000  
 Anti-mouse P27 antibody Proteintech Cat# 25614-1-AP;  
 RRID:AB\_2880161; 1:2000  
 Anti-mouse p-STAT5 antibody Cell Signaling Technology Cat# 4322;  
 RRID:AB\_10544692; 1:2000  
 Anti-mouse STAT5 antibody Cell Signaling Technology Cat# 94205;  
 RRID:AB\_2737403; 1:2000  
 Anti-mouse p-Erk antibody Cell Signaling Technology Cat# 4370;  
 RRID:AB\_2315112; 1:2000  
 Anti-mouse Erk antibody Cell Signaling Technology Cat# 4695;  
 RRID:AB\_390779; 1:2000  
 Anti-mouse Zap70 antibody Cell Signaling Technology Cat# 3165;  
 RRID:AB\_2218656; 1:2000  
 Anti-mouse p-Zap70 antibody Cell Signaling Technology Cat# 2717;  
 RRID:AB\_2218658; 1:2000  
 Anti-mouse p-4EBP1 antibody Cell Signaling Technology Cat# 2855;  
 RRID:AB\_560835; 1:2000  
 Anti-mouse p-S6 antibody Cell Signaling Technology Cat# 4858;  
 RRID:AB\_916156; 1:2000  
 Anti-mouse Actin antibody Cell Signaling Technology Cat# 3700; Lot: 18;  
 RRID:AB\_2242334; 1:2000  
 Anti-rabbit IgG, HRP-linked Antibody Cell Signaling Technology Cat# 7074;  
 RRID:AB\_2099233; 1:10000  
 Anti-mouse IgG, HRP-linked Antibody Biodragon Cat# BF03001; Lot: KIA9033285; 1:10000

## Validation

The validation of all of the antibodies depends on product datasheet and published literature.

## Eukaryotic cell lines

Policy information about [cell lines](#)

Cell line source(s) HEK293T cells were purchased from ATCC (ATCC CRL-3216).

Authentication No method of cell line authentication was used.

Mycoplasma contamination All cell lines are tested negative for mycoplasma contamination.

Commonly misidentified lines (See [ICLAC](#) register) No such cell lines were used in this study.

## Animals and other organisms

Policy information about [studies involving animals](#); [ARRIVE guidelines](#) recommended for reporting animal research

### Laboratory animals

Trmt61a-floxed mice were generated at the Shanghai Biomodel Organism Science & Technology Development Co., Ltd using the CRISPR–Cas9-based genome-editing system. The guide RNA (gRNA) and donor oligonucleotides used were listed as follows. For Trmt61a left side loxP: 5'-TGCATGAACCATGTTGTCGG-3', and 5'-AGCACACCTTTAAGCACAGTATTTGTTAGGCAGAGCAGGCAGATCTCTGGGTCTGAGACCAGCCTGATCTACATAGTGAGTTCCAGGCAGCCAAGGCTATATAGGGAGGCTGTCTGAAAGACAAAATATAGCCCTGCATGAACCATGTTGTCGGTATGATGTTACACAAATTAGCTTTCTGTTCCCATCTGTAAAGTGGTCATAAAAATTGTAAGGAAGAGGATTCAATGACATGAGAG-3'; for Trmt61a right side loxP: 5'-GTGCCCTATGAGGTCGGAGC-3', and 5'-TGGGAGCTAACCTGGGTTGGAGAAGAAAGAGGAGGAGGTGCCCTATGAGGTCGGAGCTGGGATTGCTGTATGCTGGCCAAAGGTGCTGACTGCTTTTTCTAGGCCAGCTGCCCTTCTGGAGGGAGGCTGGATACTCCAGAGCTCATTGCAGAGAGAAGTCTGTCCACACTTACAGCCAGGCCCTTCCCTAGTCCATCGAAGATTAGCACTGTCACTGATACGAGGCCAGGTGGTA-3'.

Trmt6-floxed mice were generated at the Cyagen Biosciences Inc. using the CRISPR–Cas9-based genome-editing system. The guide RNA (gRNA) and donor oligonucleotides used were listed as follows. For Trmt6 left side loxP: 5'-AAGAGACTGAGATCTCCGATAGG-3', and 5'-GCTTGTCTTTGAAGTTGCTCTAAGAGACTGAGATCTCCGATAGGAAGGCTAATGCCTGACCCTTGGCAGTACTTCATTAGTTCTACATCCATTTCCAA TGTGTAGATTGCCAATAATGTTTATTCTGACACAGGCTTTTGGAAATTTGCTTTTCTAATAGAGTAGCCAATTAGACAGA-3'; for Trmt6 right side loxP: 5'-ATGCTAGAGAATTAGCCCAACGG-3', and 5'-CTTATCTCAAAAAGGATCTTTCAGGATGCTAGAGAATTAGCCCAACGGTAAAAGTACTTGTTCCTCTGAGAAGATCCAGGTTTCAGTTCTGAACAC CCACATGGTGGCTACAACCATCTGTACTTCAGTCCAGGGATCTGATGCCCTTCTGAGCTCAGGCACCAGGCATGCATCTGGTACTCATACTG CACACAGGCAAAACTCAA-3'.

Trmt6/61aflox/flox mice were crossed with Cd4Cre mice to obtain conditional knockout mice. Cd4Cre mice were purchased from the Jackson laboratory and have been fully backcrossed to C57BL/6 mice (over more than 10 generations). RiboTag (B6N.129 strain) mice are viable and fertile, with a targeted mutation of the ribosomal protein L22 (Rpl22) locus harboring a loxP-flanked wildtype C-terminal exon 4 followed by an identical C-terminal exon 4 that is tagged with three copies of the hemagglutinin (HA) epitope before the stop codon. Prior to exposure to Cre recombinase, RiboTag mice express the wildtype RPL22 protein (15 kDa). When the RiboTag mice are bred to cre-expressing mice, offspring will have the floxed wildtype exon 4 deleted in the cre-expressing tissue and subsequent use of the downstream HA epitope-tagged exon 4 as the terminal exon. RiboTag mice were purchased from the Jackson laboratory (Strain #:011029).

Mice were housed in specific pathogen-free facility under 12h light/dark cycle at 25°C and analyzed between six to twelve-weeks of age unless described otherwise. Female and male mice were used.

### Wild animals

No wild animals were used in the study.

### Field-collected samples

No field-collected samples were used in this study.

### Ethics oversight

Animal procedures were approved by the Institutional Animal care and Use Committee (IACUC) of Shanghai Jiao Tong University School of Medicine.

Note that full information on the approval of the study protocol must also be provided in the manuscript.

## Flow Cytometry

### Plots

Confirm that:

- The axis labels state the marker and fluorochrome used (e.g. CD4-FITC).
- The axis scales are clearly visible. Include numbers along axes only for bottom left plot of group (a 'group' is an analysis of identical markers).
- All plots are contour plots with outliers or pseudocolor plots.
- A numerical value for number of cells or percentage (with statistics) is provided.

### Methodology

#### Sample preparation

Thymus, spleen, peripheral and mesenteric lymph nodes were collected and pressed through a 200- gauge mesh. Spleen cells were prepared by lysing the erythrocytes with red blood cell lysis buffer (Thermo Fisher Scientific). Primary T cells were isolated from the spleen and lymph nodes of age-matched WT and conditional knockout mice (6-12 weeks old). Naive CD4+ or total CD4+ T cells were purified by using EasySep Mouse Naive CD4+ T or CD4+ T Cell Isolation Kit (STEMCELL Technologies) according to the instructions, respectively.

#### Instrument

Flow cytometry data were collected with a BD Fortessa X20 (BD FACSDiva Software v8.0.1). Flow sorting was performed using an Arial III (BD Biosciences)

#### Software

Flow cytometry data were analyzed using the FlowJo (vX.0.7).

#### Cell population abundance

20,000-100,000 cells were acquired and analyzed for each independent experiment.

#### Gating strategy

Cells were first gated on CD45+ population, and then gated on FSC/SSC, doublets excluded by

Gating strategy

T cells were identified by gating CD3+TCRb+ cells. CD4 and CD8 T cells were identified by gating CD4+ and CD8+ events within the CD3+TCRb+ gate.

Tick this box to confirm that a figure exemplifying the gating strategy is provided in the Supplementary Information.